

上海交通大学

SHANGHAI JIAO TONG UNIVERSITY

学士学位论文

BACHELOR'S THESIS



论文题目：基于无线信号时间相关性的室内定位技术研究

学生姓名：_____ 王玫

学生学号：_____ 5120309691

专 业：_____ 信息工程 (IEEE)

指导教师：_____ 田晓华

学院(系)：_____ 电子信息与电气工程学院

Submitted in total fulfillment of the requirements for the degree of Bachelor
in Information Engineering (IEEE)

TEMPORAL CORRELATION OF RSS IMPROVES ACCURACY OF FINGERPRINTING LOCALIZATION

MEI WANG

Advisor

Prof. XIAOHUA TIAN

DEPARTMENT OF ELECTRONIC ENGINEERING

SCHOOL OF ELECTRONIC INFO. & ELECTRICAL ENGINEERING

SHANGHAI JIAO TONG UNIVERSITY

SHANGHAI, P.R.CHINA

June 14th, 2016

基于无线信号时间相关性的室内定位技术研究

摘 要

近年来，利用无线信号强度的指纹室内定位方法是十分热门的研究课题。最近的一项研究成果提出了一种计算指纹定位精度基本极限的方法：对于给定的定位精度，我们可以利用似然概率计算出定位结果的可靠性。利用室内位置信息的智能系统拥有广阔的应用价值，那么高精度的室内定位需求就成了亟待解决的核心问题。因此，一个自然的问题就是：我们能否从根本上进一步提高指纹定位方法精度的极限呢？在本论文中，我们从理论上证明了利用无线信号强度的时间相关性可以提高指纹定位方法的精度。特别地，我们创建了一个广义的无线电波传播模型，加入信号时间相关因素后形成一个更为完整的指纹定位理论框架，并基于此揭示了无线信号强度的时间相关性对定位可靠性的影响。在此理论模型中，我们定义了定位系统中采样空间，物理空间及时间序列的映射关系和数学表示，并从代数几何的角度详细讨论了信号时间相关性提高定位精度的根本原因和物理意义。同时，我们还进一步探讨了定位可靠性积分区间在高维采样空间中的转换方法和空间描述。通过搭建实际的室内定位系统，实验结果充分证实了理论分析。我们不仅设计了利用时间相关信息的粗细粒度结合的定位算法，还做对照实验找到了最合理的系统关键参数。最后的实验结果显示，合理利用信号的时间相关性可以将定位精度提高达 13%。

关键词： 指纹定位，理论建模，时间相关性

TEMPORAL CORRELATION OF RSS IMPROVES ACCURACY OF FINGERPRINTING LOCALIZATION

ABSTRACT

Indoor localization based on RSS fingerprinting approach has been attracting many research efforts in the past decades. Recent study presents a fundamental limit of the fingerprinting localization approach: given requirement of estimation accuracy, reliability of the user's localization result can be derived. As highly accurate indoor localization is essential to enable many location based services, a natural question to ask is: can we further improve the accuracy of the localization scheme fundamentally? In this paper, we theoretically show that the temporal correlation of the RSS can improve accuracy of the RSS fingerprinting based indoor localization. In particular, we construct a theoretical framework to evaluate how the temporal correlation of the RSS can influence the reliability of location estimation, which is based on a newly proposed radio propagation model considering the time-varying property of signals from Wi-Fi APs. Such a theoretical framework is then applied to analyze localization in the one dimensional physical space, which reveals the fundamental reason why performance improvement of localization can be brought by temporal correlation of the RSS. We further extend our analysis to high-dimensional scenarios and mathematically depict the boundaries in the RSS sample space, which distinguish one physical location from another. Moreover, we develop an algorithm to utilize temporal correlation of the RSS to improve the location estimation accuracy, where the process for choosing key design parameters are provided through experiments. Experiment results show that the localization accuracy can be improved by up to 13% with appropriate leveraging the RSS temporal correlation.

KEY WORDS: Fingerprinting Localization, Theoretical Modeling, Temporal Correlation

Content

Figure Index	v
Table Index	vi
Symbols	vii
Chapter 1 Introduction and Related Work	1
1.1 Introduction	1
1.2 Related Work	4
1.2.1 Overview of WLAN Fingerprinting Localization	4
1.2.2 Fundamental Limits of RSS Fingerprinting Approach	6
1.2.3 Temporal Information of RSS Utilized for Localization	8
Chapter 2 Theoretical Model of Location Estimation	9
Chapter 3 Analysis of 2-D Temporal Correlation for 1-D Physical Space Localization	12
3.1 Finding Region \mathbb{E}	12
3.2 Analysis on Region \mathbb{E}	15
3.2.1 Boundaries of Region \mathbb{E}	16
3.2.2 Accurate Description of \mathbb{E}	17
3.3 Influence of Temporal Correlation on Accuracy of Localization	19
Chapter 4 High-Dimensional Extensions for Localization	21
4.1 High-Dimensional Temporal Correlation	21
4.2 High-Dimensional Sample Space	22
4.3 Two-Dimensional Physical Space	24

Chapter 5 Asymptotic Equivalent Region of \mathbb{E} in High-Dimensional Scenarios	26
5.1 Approximate Matrix	26
5.2 Asymptotical Equivalence Analysis	28
5.3 Boundaries of Region \mathbb{E}'	32
Chapter 6 Location Estimation Facilitated by Temporal Correlation of the RSS	35
6.1 Feasibility of Utilizing Temporal Correlation	35
6.2 Localization Estimation Algorithm	38
6.3 Choice of Design Parameters	40
Chapter 7 Simulation and Experiment Results	43
7.1 System Setups	43
7.1.1 Fingerprint Collection	43
7.1.2 Database and Server	44
7.1.3 Location Determination	44
7.2 Trace-driven Simulation	45
7.2.1 Simulation introduction	45
7.2.2 Simulation in 2-D PDFs with correlation	46
7.3 Evaluation and Experimental Results	48
SUMMARY	52
Bibliography	53

Figure Index

1-1	Two Phases for Fingerprinting Localization Systems	5
1-2	Graphical Illustration of Fundamental Limits Model.	7
2-1	Theoretical localization model.	10
3-1	Joint Gaussian PDF of $RSS(t)$ and $RSS(t + \tau)$ at position \mathbf{r}	13
3-2	Joint Gaussian PDFs at Different Locations.	14
3-3	Graphical illustration of region \mathbb{E}	16
3-4	Intersection of two Gaussian PDFs.	18
4-1	Region \mathbb{E} in 2-D physical space localization.	25
5-1	Simplified Region \mathbb{E} with high dimensional samplings in 2-D physical space.	34
6-1	Spatial distribution of values of ρ and μ	36
6-2	Comparison of Correlation ρ , Variance σ and Mean Value	37
6-3	Parameter analysis of the number of correlation dimensions	40
6-4	Parameter analysis of the sampling interval	41
6-5	Parameter analysis of the number of samplings	42
6-6	Comparison of correlation with different sampling number	42
7-1	PDFs of the tested RSSes	45
7-2	2-D Gaussian Distribution and Hyperbolic Criteria for Localization	47
7-3	Reliability with different threshold H and error tolerance radius	50

Table Index

7-1	RSS results fitting 1-d Gaussian parameters	45
7-2	RSS results fitting 2-D Gaussian parameters.	46
7-3	Combination of H and radius and corresponding reliability improvement	51

Symbols

- L Physical Space (All possible reference points)
- \mathbf{r} Position vector of user in physical space
- \mathbf{r}' Estimated Position of user in physical space
- Q Localization Area
- δ Localization Radius
- θ The angle between \mathbf{r} and δ
- Ω^n All possible outcomes (RSSes)
- n The number of Access Points (APs)
- w Sample times for each AP
- $x_{i,j}$ RSS observation with respect to AP_i at j_{th} time point
- M Mapping from the sample space to the physical space
- $\mathbf{X}(\mathbf{r}, t)$ Random variable for RSS measurements
- $\mathbf{S}(\mathbf{r}, t)$ Random variable of the residential part
- $\mathbf{Y}(\mathbf{r}, t)$ Colored Noise
- \mathbf{t} The vector of time slots
- σ_t Localization Area
- \mathbb{E} The region in Sample Space where the user's location can be estimated to be in Q
- $R()$ Localization Reliability represents the probability of reported RSSes fall in E
- $f(x_i)$ Probability density function of RSS measurements
- τ Time duration
- μ Mean value of RSS
- σ Standard variance of RSS
- ρ Auto-correlation coefficient of function f

- Δ The Mahalanobis distance
- Σ Covariance matrix of function f
- \mathbf{y} New variance in rotated coordination system
- λ Engenvalue
- \mathbf{u} Eigenvector
- \mathbf{J} Jacobian Matrix
- m Temporal Dimension
- Th Threshold parameter
- t RSS Testing time

Chapter 1 Introduction and Related Work

1.1 Introduction

Indoor localization based on Received Signal Strength (RSS) fingerprinting approach has been attracting many research efforts in the past decades, where the basic idea is to first construct RSS fingerprints database during the training phase, and then perform location estimation by matching the user's reported fingerprints in the database during the localization phase [1]. Indoor localization systems based on the approach have been developed with different flavors. Embedded sensors of mobile devices are exploited to improve accuracy of the location estimation [2, 3], crowdsourcing paradigm is used to reduce the cost of site survey in the training phase [4], and machine learning algorithms are leveraged to shorten the delay of localization process [5, 6, 7].

The spring-up of RSS fingerprinting based indoor localization systems promotes efforts to study performance bounds of such systems both empirically and theoretically. Empirical studies evaluate performance of localization systems with comprehensive experiments. Liu *et al.* present their experimental results showing that the location estimation error could be over 6m [2]. Chandrasekaran *et al.* provide empirical quantification of accuracy limits of RSS localization, which is based on extensive experimental results conducted over a uniform testbed [8]. Such results could be helpful references for system implementation but hardly provide insight into the RSS fingerprinting approach. Some theoretical studies about localization performance bound are based on Cramér-Rao Bound (CRB) analysis [9, 10, 11]; however, that framework is based on the Log-Distance Path Loss (LDPL) radio propagation model [1, 8], which however has been proved inaccurate in the indoor localization scenarios [12].

Recently, Wen *et al.* present a theoretical investigation on RSS fingerprinting based indoor localization, which reveals fundamental limits of the localization methodology [13]. Specifi-

cally, the work derives a close-form expression for calculating the probability that a user can be correctly localized in a region of certain size, which is termed as localization reliability. The basic idea of the derivation is to build a probability space induced from RSS samples obtained from the training stage. The location determination process can be regarded as a mapping from the sample space to the physical space; therefore, the probability a user can be correctly localized in a certain region is equal to the probability that certain outcomes of RSS measurements appear, so that the localization system can determine the user's location to be in the region. As highly accurate indoor localization is essential to enable many location based services, a natural question to ask is: can we further improve the performance of the localization scheme fundamentally?

In this paper, we show that the temporal correlation of the RSS can improve accuracy of RSS fingerprinting based indoor localization. We first construct a theoretical framework to analyze how the temporal correlation of the RSS can influence the accuracy of location estimation, which is based on a newly proposed radio propagation model considering the time-varying property of signals from given Wi-Fi Access Points (APs). Based on such a model, we build a new sample space from the training phase, where each outcome in the space is extended with a new temporal dimension. With such a framework, we can leverage new extra fingerprints to estimate the user's location, which are actually the temporal correlation of the RSSes observed from the APs.

We then apply the theoretical framework to analyze the localization process in the one-dimensional physical space, which reveals the fundamental reason why performance of localization can be improved by leveraging temporal correlation of the RSS. An interesting finding is that: the boundary in the sample space used to distinguish one physical location from another, in fact should be one edge of hyperbola, instead of a line as believed in most of the work in the literature; moreover, we find that the curvature of the hyperbola is related to the correlation of the RSS in the sample space. Such finding can fundamentally improve accuracy of location estimation of the RSS fingerprinting based system.

We extend our analysis to high-dimensional scenarios, where high temporal and sample space dimensions, and two-dimensional physical space are taken into account. The major chal-

length for the high-dimensional case is to deal with the complicated relationship between the location in the physical space and the corresponding temporal correlation of the RSS in the sample space. We firstly derive a transformation matrix, which represents the linear affine transformations in Euclidean space like translation, rotation, and shearing, to deal with the challenge. We theoretically prove that the boundary in the sample space dividing two physical locations is a high-dimensional hyperbolic plane. To be more precisely, we propose to approximate the covariance matrix of the RSS in a location with a simplified matrix, which enables finding the boundaries that are asymptotically equivalent to the original ones. We then mathematically depict the boundaries in the sample space that distinguish the one physical space from another in the high temporal, sample space and physical space dimensions.

Further, we develop an algorithm to improve performance of the location estimation utilizing temporal correlation of the RSS. The basic idea is using the mean of the RSS to find a list of candidate locations the user could be currently at, and then leveraging the temporal correlation to choose the best estimation on the list. We conduct experiments to show the feasibility of the algorithm and choose key design parameters for the algorithm. We also apply the algorithm in the practical location estimation process, and the results show that the localization accuracy can be improved by up to 13% with appropriate leveraging the RSS temporal correlation.

The remainder of the paper is organized as follows. Section 1.2 presents related work. Chapter 2 illustrates the service model. Chapter 3 presents our analysis of localization with one-dimensional physical space, sample space and two-dimensional temporal space. Chapter 4 shows how to extend our analysis to higher dimensional cases. Chapter 5 mathematically depicts boundaries in the sample space to distinguish one physical location from another. Chapter 6 presents a localization algorithm leveraging the temporal correlation to improve accuracy of location estimation. Chapter 7 presents trace-driven simulations, system setups and experimental results. The conclusion remarks and future work are provided in the Summary part.

1.2 Related Work

Recently communication systems increasingly rely on Location-based Services (LBS), such as healthcare monitoring [14], personalized information delivery [15] and so on. While outdoor localization services are well served by Global Positioning System (GPS) for decades, indoor localization still remains an open problem because of complicated indoor environments. The reflections from indoor obstacles, the delay of signal readings, the non-line-of-sight (NLOS) propagations all lead to a multi-path signal profile [16], which make the indoor positioning problem more challengeable than that in outdoor scenarios.

To tackle the indoor positioning task, many indoor localization techniques and sophisticated schemes are developed utilizing deployed sensors [17], RFID [18], Bluetooth [19], infrared transceivers [20], etc. However, considering the deploying and maintaining costs, these methods are inferior to the Wireless Local Area Networks (WLAN) positioning approaches. Such WLAN localization technologies can roughly categorized into two groups: the deterministic methods – Angle of Arrival (AOA) [21], Time of Arrival (TOA) [22] or Time Difference of Arrival (TDOA) [23], and the probabilistic methods – Fingerprinting method [6, 7, 9].

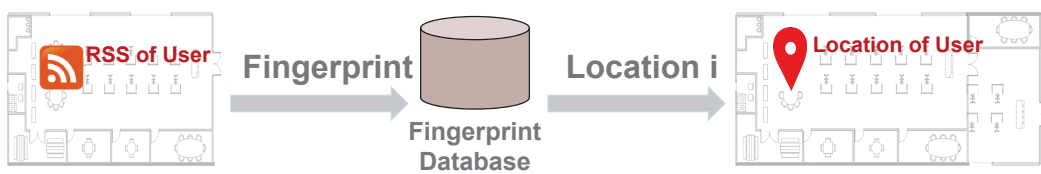
1.2.1 Overview of WLAN Fingerprinting Localization

Among all the aforementioned positioning schemes, fingerprinting method has gathered much attention. The basic idea of fingerprinting approach can be described as two phases shown as Fig. 1–1. First in the offline phase, we divide the physical area into grids and make them as location Reference Points (RP). And then collect a number of RSSes of all detected WLAN APs at each reference point to make the RSS profiles as radio map. On the other hand, the online phase is to estimate the user’s location by matching the request measurement and radio map. Typically, there are many positioning algorithms for the online localization phase, like k-Nearest Neighbor (kNN), Machine Learning (ML), Compressive Sensing (CS), etc.

Take the Fig. 1–1 for a specific example. There are four reference points and three visible WLAN access points in this office area. Notice that fingerprinting techniques do not rely on known AP positions and do not attempt to get AP-to-user distances from RSS profiles. In the



(a) Offline Training Phase of Fingerprinting Localization System



(b) Online Localization Phase of Fingerprinting Localization System

Figure 1–1: Two Phases for Fingerprinting Localization Systems

offline phase, we can use smartphones to collect the RSS fingerprints at all reference locations. And then send the fingerprint collection to the database. The raw RSS data would be preprocessed to make a radio map, typically we use the mean value of the RSSes of each AP to fit Gaussian distribution as the radio map. When a user wants to find where he is and send a request message with tested RSSes to the server, the RSS data will be compared with the database and find the most probable one reference point. Finally the system sends back the position of the proposed RP to the user.

There are many challenges for the fingerprint localization approach. First of all, as mentioned before, in such complicated indoor circumstance, the reflection, obstruction and non-line-of-sight propagation lead to a multipath signal profile [16], which makes the user's location indirectly predictable from RSS data. Second, the signal strength of an AP fluctuate itself randomly. In addition to the power control and frequency management policy, all of these make their recognition and association with RPs more complex. Third, although mostly we assume the RSS fingerprints is Gaussian or Multi-Gaussian distributed, the actual distribution is more likely non-Gaussian, skewed, multimodal and time varying. What's more, there are still some other influential factors, like the different versions of users' smartphones, the decay of reading

signals, the motion of pedestrian, all of which make the RSS profile inconsistent.

To tackle the aforementioned challenges and improve the localization accuracy, increasing number of studies focus on all kinds of problems in fingerprinting localization system. In order to save the cost of arduous fingerprint collection and indoor map drawing jobs, someone use robots to do it automatically. Rai *et al.* present *Zee* [24] to utilize crowdsourcing technology to collect the training data without any explicit effort on the part of users. Some other works exploit more from the supplemental sources of information, like the *UnLoc* system developed by Wang *et al.* [25]. They use mobile devices to sense the identifiable signatures as natural landmarks, like elevator. With the help of dead-reckoning schemes, they can realize unsupervised indoor localization system with little deployment. Another exciting work of Kumar *et al.* named *Ubicarse* [26], which enables handheld devices to emulate large antenna arrays using a new formulation of Synthetic Aperture Radar (SAR) and make centimeter-level localization accuracy with zero start-up cost.

Towards the WLAN positioning algorithms, Youssef *et al.* [27] proposed one of the earliest fingerprinting schemes. They select a subset of the strongest APs and this is also common these days. Kushki *et al.* [28] proposed a kernel-based WLAN positioning scheme utilizing spatiality information to improved positioning results. Recently Compressive Sensing (CS) approach [29] leveraging sparse signal processing techniques gets much more popular.

1.2.2 Fundamental Limits of RSS Fingerprinting Approach

Wen *et al.* present a theoretical investigation on RSS fingerprinting based indoor localization, which reveals fundamental limits of the localization methodology [13]. Specifically as Fig. 1–2, if a user's real location is at Q , the work derives a close-form expression of the probability R that the user can be localized in the δ neighborhood of Q , where δ and R are localization accuracy and reliability, respectively.

With the RSS fingerprinting based localization approach, RSS fingerprints obtained from the training stage form a sample space, based on which a user's location in the physical space can be estimated. The location determination process can be regarded as a mapping from the sample space to the physical space. If outcomes of RSS measurements fall into the event region

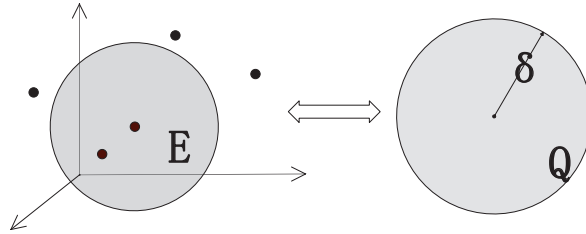


Figure 1–2: Graphical Illustration of Fundamental Limits Model.

\mathbb{E} , then the localization system can correctly determine the location of the user to be in the δ neighborhood of Q ; therefore, the localization reliability is equal to the probability that outcomes of RSS measurements fall into the event region \mathbb{E} . By constructing a general radio propagation model based on field observations of real localization systems, probabilities for outcomes of RSS measurements in a location can be presented, which turns out to be following Gaussian distribution. Consequently, calculating the localization reliability is to first find the event region \mathbb{E} in the RSS sample space, and then perform integration over the region \mathbb{E} for an Gaussian probability density function (PDF).

Although utilizing a general radio propagation model, the study in [13] is distinguishable from the model based localization because the radio propagation model is not used to derive geometric relationships between signal transmitters and receivers, such as distance, time of arrival (ToA), time difference of arrival (TDoA) or angle of arrival (AoA) [1]. That is why the radio propagation model used in [13] only assumes that the mean of RSS readings varies with respect to locations but does not specify how the mean will vary. This is in contrast to the Log-Distance Path Loss (LDPL) model used in the model based localization and CRB analysis [9, 10, 11], where the mean varies with respect to locations logarithmically. Moreover, interesting findings about the shape of the event region \mathbb{E} are presented in [13], where skillful mathematical techniques are demonstrated. We note that efforts have been made to estimate the user's location with channel state information (CSI) [30, 31, 26]; however, this category of work is highly dependent on the device [32] that provides the CSI. In practice, the CSI is still not provided by most if not all of manufacturers to the best of our knowledge.

Our study constructs a new radio propagation model considering the temporal correlation

of the RSS, which is not taken into account in [13]. The later discussions are to reveal that the boundary distinguishing one location from another in the sample space is different from that shown in [13], and the new boundary provides a more accurate location estimation. Compared with the pure theoretical analysis presented in [13], we present experimental results to validate our theoretical analysis.

1.2.3 Temporal Information of RSS Utilized for Localization

Kaemarungsi *et al.* study properties of the RSS for fingerprinting based localization using Wi-Fi [33]. Comprehensive experiment results reveal two important features of the RSS: First, the mean and variance of the RSS in one location basically remain the same over time; second, the auto-covariance function of the RSS in one location has the same shape for separate time-series. Based on such two observations, our work in this paper models the RSS observed in one location as a stationary process. Youssef *et al.* found in [34] that the autocorrelation between consecutive samples from the same access point can be as high as 0.9. Their *Horus* system shows that the average system accuracy is increased by more than 50%, and wrong assumption of independence of samples from the same access point can lead to degraded performance. Fang *et al.* propose a localization approach based on the dynamic system and machine learning technique[6]. Such an approach estimates the user's location by the state consisting of RSSes observed in different times and locations. However, the simple combination of spatial and temporal information does not reveal the essence how the temporal information can be utilized for localization, where the RSS observed in different times can be considered as multiple measurements of fingerprints.

Most of the current studies for utilizing temporal information of the RSS for localization are in a machine-learning based manner [5, 7], where the convincing explanation how the temporal information can influence the performance of the localization process is still unavailable. In this paper, we initiate the theoretical study on this issue.

Chapter 2 Theoretical Model of Location Estimation

Consider an indoor space, which can be modeled as one or two dimensional Cartesian space denoted by $L \subset \mathbb{R}$ or $L \subset \mathbb{R}^2$, respectively. Examples of one dimensional model include hallway and corridor. A user's location in the physical space S can be denoted by $\vec{r} = r_1$ or $\vec{r} = (r_1, r_2)$ with corresponding dimensions. Based on the localization database constructed in the training phase, a sample space of fingerprints can be induced, which is denoted by Ω^n and n is the number of access points (APs) can be sensed in the physical space. In the training phase, the site surveyor collects fingerprints of APs in a one-by-one manner at a given location. For an AP, the surveyor samples the observed RSS at certain frequency. Consequently, if there are n APs and each AP is sampled w times, then a point \mathbf{x} in the RSS sample space is in the following form:

$$\begin{bmatrix} x_{1,1} & x_{1,2} & \dots & x_{1,w} \\ x_{2,1} & x_{2,2} & \dots & x_{2,w} \\ \vdots & \vdots & \ddots & \vdots \\ x_{n,1} & x_{n,2} & \dots & x_{n,w} \end{bmatrix}$$

, where $x_{i,j}$ means the RSS observed with respect to AP_i at j th time point. We say this is an n -dimensional sample space and the temporal dimension of sampling is w .

As the radio propagation in the indoor environment is influenced by many factors such as path loss, shadowing, fading and multi-path effect, the signal can be observed in a location is usually modeled as a random process, which can be denoted as

$$X(\vec{r}, \vec{t}) = S(\vec{r}) + \sigma Y(\vec{r}, \vec{t}), \quad (2-1)$$

where \vec{r} is the location of the observation and \vec{t} represents the vector of time points at which RSSes are observed. $S(\vec{r})$ is the trend model of the signal with respect to position \vec{r} in the

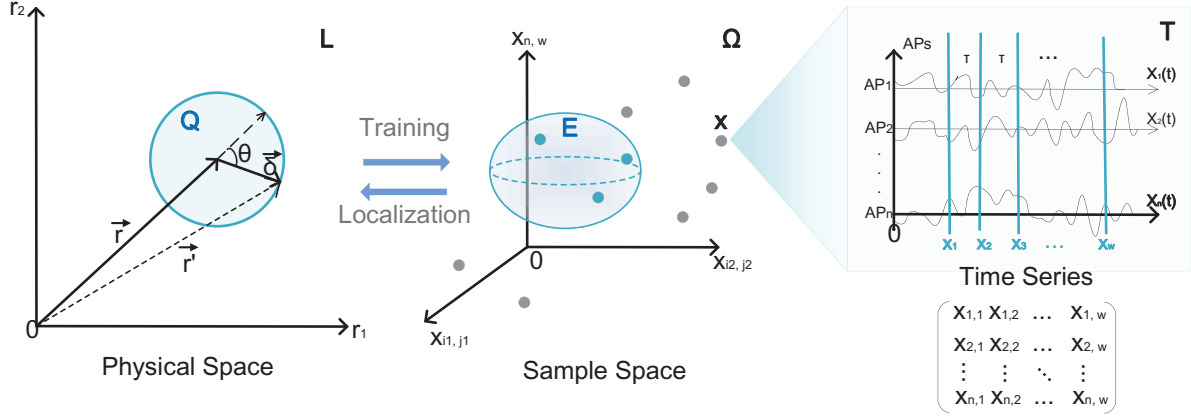


Figure 2–1: Theoretical localization model.

perspective of stochastic processes, and σ is the amplitude of noise. $Y(\vec{r}, \vec{t})$ is the joint Gaussian distribution of temporal noise series at location \vec{r} .

According to extensive experimental results and theoretical analysis [35, 36, 12], the mean and variance of the RSS in one location basically remain the same over time and the auto-covariance function of the RSS in one location has the same shape for separate time-series, such a random process can be stationary and ergodic, with

$$S(\vec{r}') \approx S(\vec{r}) + \nabla S(\vec{r})(\vec{r}' - \vec{r}) \quad (2-2)$$

In the localization phase, a user reports observed RSSes to the localization server, which then estimates the corresponding location by matching the reported fingerprints in the fingerprints database. Such a process can be modeled as a mapping from the sample space to the physical space:

$$M : \Omega^n \rightarrow L, \quad \mathbf{r}' = M(\mathbf{X}(\vec{r}, \vec{t})), \quad (2-3)$$

where \vec{r}' is the estimated location of the user. This process is illustrated in Fig. 2–1. The user's actual location is at \vec{r} and the estimated location is at \vec{r}' , which incurs the localization error denoted by $\vec{\delta}$.

Due to estimation errors, the result of the localization is that the user's location is estimated to be in the δ neighborhood of \mathbf{r} , which is denoted by Q . To reduce the error of localization

is equivalent to mitigating the norm of $\vec{\delta}$. Since the basis of the estimation is the reported fingerprint by the user, the ideal case is that the user's submitted fingerprints happen to make the system believe that the location of the user is in Q . We use \mathbb{E} to denote such a region in the sample space, so that the user's location can be estimated to be in Q as long as the reported RSSes fall in \mathbb{E} .

The probability that the reported RSS fingerprints can fall into the region of \mathbb{E} depends on the model of radio signal propagation, which in fact fundamentally determines the performance of the RSS fingerprinting based approach. The model proposed in [13] considers the observed RSS at one location as a random variable, where temporal correlation of the signal is not taken into account. According to the site survey practice, it is more practical to model the signal as a random process as in this paper, where the temporal correlation can be leveraged. Our investigation in the rest of the paper is to show that such a seemingly slight change in the radio signal propagation modeling brings about not only much higher difficulties in mathematical analysis, but also interesting findings of the RSS fingerprinting based approach, which have never been revealed.

Chapter 3 Analysis of 2-D Temporal Correlation for 1-D Physical Space Localization

This chapter examines a concrete scenario of localization, where both the physical space and the sample space are one dimensional and the temporal dimension of sampling is two. The purpose of the examination is to find how likely the user can be localized in Q with given δ . It is easier to reveal essence of the fingerprinting approach by analyzing a simple case, where the results could be inspiring for analyzing more complicated scenarios.

3.1 Finding Region \mathbb{E}

Let us first find out what kind of RSSes can be observed at the location \mathbf{r} . The one-dimensional physical space can be regarded as an one-dimensional horizontal axis, where the origin of the axis is the location of the AP, and the location of each point can be identified by a scalar r . Based on our proposed radio signal propagation model, the probability density function (PDF) of RSS readings can be observed follows the Multivariate Gaussian Distribution, which is denoted by

$$f_r(x_1, x_2) = \frac{1}{2\pi\sigma^2\sqrt{1-\rho^2}} e^{-\frac{1}{2}\Delta^2}, \quad (3-1)$$

where x_1, x_2 are variables representing the RSSes at time points t_1 and t_2 separated by a duration of τ . Figure 3-1 illustrates $f_r(x_1, x_2)$. Since the random process representing the signal is stationary, the following analysis is oblivious to the specific value of t_1 and t_1 as long as they are separated by τ . Symbols μ and σ are the mean and standard variance of the RSS joint distribution at position \mathbf{r} , respectively; ρ is the autocorrelation coefficient of $f_r(x_1, x_2)$. The

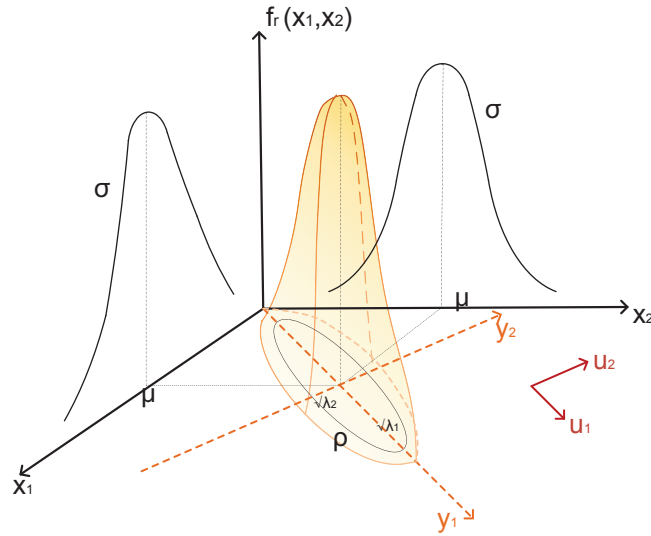


Figure 3–1: Joint Gaussian PDF of $RSS(t)$ and $RSS(t + \tau)$ at position \mathbf{r}

Mahalanobis distance is denoted as Δ , where

$$\Delta^2 = \frac{1}{\sigma^2(1 - \rho^2)} [(x_1 - \mu)^2 + (x_2 - \mu)^2 - 2\rho(x_1 - \mu)(x_2 - \mu)]. \quad (3-2)$$

Since x_1 and x_2 are both observed at r , the corresponding marginal distributions with respect to x_1 and x_2 are the same, according to our signal propagation model, and the corresponding means and standard variances of the two marginal distributions are the same as well. This also complies with the conclusion in [13]. Consequently, the covariance matrix of $f_r(x_1, x_2)$ is real, positive and symmetric, where

$$\Sigma = \sigma^2 \begin{bmatrix} 1 & \rho \\ \rho & 1 \end{bmatrix}. \quad (3-3)$$

With the same reason, the major axis of the elliptical surface representing $f_r(x_1, x_2)$ should be the angular bisector of the Cartesian coordinates with slope 1.

In order to facilitate our analysis, we put the image of $f_r(x_1, x_2)$ in a new coordinates system with axes y_1 and y_2 . We let the major axis of the elliptical surface align to y_1 and the origin of the new coordinates system be $(\mu(r), \mu(r))$ in the old system. Then the PDF in the new system

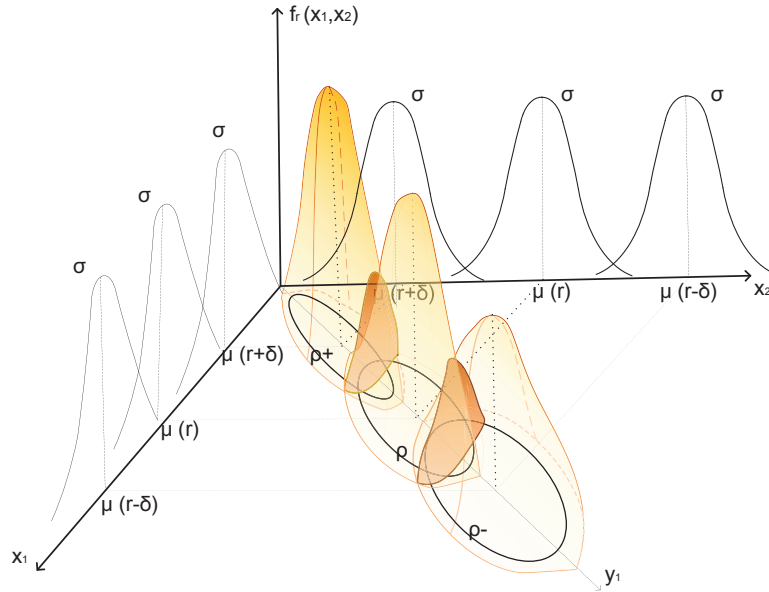


Figure 3–2: Joint Gaussian PDFs at Different Locations.

is

$$f_r(y_1, y_2) = \frac{1}{2\pi\sigma^2\sqrt{\lambda_1\lambda_2}} e^{-\frac{1}{2\sigma^2}\left(\frac{y_1^2}{\lambda_1} + \frac{y_2^2}{\lambda_2}\right)}, \quad (3-4)$$

where

$$\lambda_1 = \frac{\sqrt{2}(1 + \rho)}{2}, \lambda_2 = \frac{\sqrt{2}(1 - \rho)}{2}. \quad (3-5)$$

We now start to find the region \mathbb{E} in this scenario. Refer to Fig. 3–2, the value of $f_r(y_1, y_2)$ in fact means how likely the user can observe $[y_1, y_2]$ at location r . If the reported RSSes $[y_1, y_2]$ indicate that the user’s location is in a small neighborhood of r , then $f_r(y_1, y_2)$ should be higher than $f_{r\pm\delta}(y_1, y_2)$, where $r \pm \delta$ are boundaries of r ’s neighborhood in the physical space. That is, if the user is localized in the neighborhood of r , the corresponding submitted fingerprints should have fallen into the region

$$\mathbb{E} = \{\mathbf{x} | f_r(\mathbf{y} | \mu(r), \Sigma(r)) \geq f_{r\pm\delta}(\mathbf{y} | \mu(r \pm \delta), \Sigma(r \pm \delta))\}. \quad (3-6)$$

The profile of \mathbb{E} is sketched in Fig. 3–2, which is the space between the two regions in dark color. The two dark-colored regions themselves represent boundaries of intersected neighboring dome-like bodies. Observe marginal PDFs with respect to x_2 for the three locations $r - \delta, r$

and $r + \delta$, which are presented by three Gaussian PDF curves on the $x_2 - f(x_1, x_2)$ plane with means $\mu(r - \delta)$, $\mu(r)$ and $\mu(r + \delta)$, respectively. It is worth mentioning that shapes of the three curves are the same, which is determined by the variance of Gaussian noise. This is because Gaussian noise at different locations in a small neighborhood of the physical space are presenting indistinguishable randomness, which have been acknowledged by extensive studies [33, 13]. Due to symmetry of the dome-like bodies, the same thing happens to the marginal PDFs with respect to x_1 .

If the temporal correlation of the RSS is not considered, fingerprints can be observed at different time points with respect to the same AP are independent at each location; therefore, the randomness of the RSS can only be characterized in a 2-D curve of the marginal PDF as shown in Fig. 3–2. Using such randomness to evaluate the performance limit of fingerprinting localization is the basic idea in [13].

Our work in this paper characterizes randomness of the RSS with the dome-like bodies as shown in Fig. 3–2, where the temporal correlation of the signal is taken into account. We can see that our model presents a more accurate description of the randomness of the RSS, where a straightforward observation is the increase of a dimension. Such a model of the RSS provides more distinguishable characteristics of a location compared with that in [13], thus provides criteria of finer-granularity for localization. This is the fundamental reason why the accuracy performance bound of localization derived in [13] can be further improved if the RSS temporal correlation is taken into account.

3.2 Analysis on Region \mathbb{E}

Since the location estimation is performed based on fingerprints reported by the user, studying properties of \mathbb{E} can help reveal how the system estimates the user's location. Intuitively, if we project the image in Fig. 3–2 onto the $y_1 - y_2$ coordinates system, the resulted image should be that as shown in Fig. 3–3. The region in yellow should be the projection of the space \mathbb{E} , and the two curves in yellow should be boundaries of the region. Consequently, if a user's reported fingerprints fall into the area left to \mathbb{E} , the user is more likely at the location $r - \delta$; if the reported

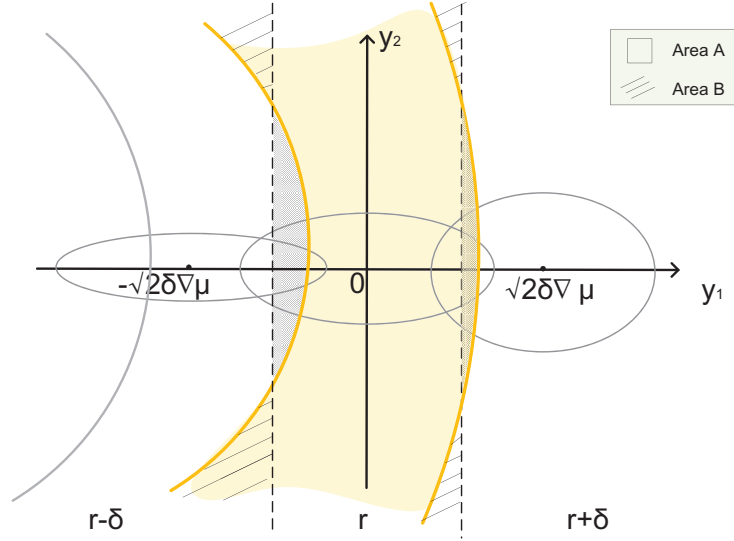


Figure 3-3: Graphical illustration of region \mathbb{E}

fingerprints fall into the area right to \mathbb{E} , the user is more likely at the location $r + \delta$. We are to reveal that the boundaries of \mathbb{E} are in the shape of hyperbolic curve with interesting properties, and then reveal challenges for accurately describing the region \mathbb{E} with corresponding analysis provisioned.

3.2.1 Boundaries of Region \mathbb{E}

Substituting Eq. (3-4) into Eq. (3-6), we obtain the following inequality:

$$\frac{1}{\sqrt{\lambda_1 \lambda_2}} e^{-\frac{1}{2\sigma^2} \left(\frac{y_1^2}{\lambda_1} + \frac{y_2^2}{\lambda_2} \right)} \geq \frac{1}{\sqrt{\lambda_1^\pm \lambda_2^\pm}} e^{-\frac{1}{2\sigma^2} \left(\frac{(y_1 \pm \sqrt{2\delta} \nabla \mu)^2}{\lambda_1^\pm} + \frac{y_2^2}{\lambda_2^\pm} \right)}, \quad (3-7)$$

where λ_1, λ_2 are scaling factors of ellipse axes for Gaussian PDF at position r , and $\lambda_1^\pm, \lambda_2^\pm$ are scaling factors at adjacent positions $r \pm \delta$. Specifically,

$$\begin{aligned} \lambda_1 &= \frac{\sqrt{2}(1+\rho)}{2}, \lambda_2 = \frac{\sqrt{2}(1-\rho)}{2}; \\ \lambda_1^\pm &= \frac{\sqrt{2}(1+\rho^\pm)}{2}, \lambda_2^\pm = \frac{\sqrt{2}(1-\rho^\pm)}{2}. \end{aligned} \quad (3-8)$$

Symbols ρ, ρ^\pm are the autocorrelation coefficients for the Gaussian distribution at r and $r \pm \delta$, respectively. After simplification, they are equivalent to:

$$\begin{cases} \left(\frac{y_1^2}{\lambda_1} + \frac{y_2^2}{\lambda_2} \right) - \left(\frac{(y_1 + \sqrt{2}\delta \nabla \mu)^2}{\lambda_1^+} + \frac{y_2^2}{\lambda_2^+} \right) \leq \ln \frac{\lambda_1 \lambda_2}{\lambda_1^+ \lambda_2^+}; \\ \left(\frac{y_1^2}{\lambda_1} + \frac{y_2^2}{\lambda_2} \right) - \left(\frac{(y_1 - \sqrt{2}\delta \nabla \mu)^2}{\lambda_1^-} + \frac{y_2^2}{\lambda_2^-} \right) \leq \ln \frac{\lambda_1 \lambda_2}{\lambda_1^- \lambda_2^-}, \end{cases} \quad (3-9)$$

which is the specific expression of \mathbb{E} in the sample space. The boundaries of \mathbb{E} can be obtained when the equality holds.

In order to better understand properties of the boundaries, we transform the expressions in inequalities (3-9) into a general form

$$Ay_1^2 + By_1y_2 + Cy_2^2 + Dy_1 + Ey_2 + F = 0, \quad (3-10)$$

where the discriminant Δ equals to

$$\Delta = B^2 - 4AC, \quad (3-11)$$

and $A = \frac{1}{\lambda_1} - \frac{1}{\lambda_1^\pm}$, $C = \frac{1}{\lambda_2} - \frac{1}{\lambda_2^\pm}$. Since $B = 0$, $AC < 0$, then $\Delta > 0$. This means that the two boundaries of \mathbb{E} are in the shape of the hyperbolic curve, where the two foci are on axis y_1 .

Note that if $A = C$ and $B = 0$, both of the boundaries are straight lines in parallel. $A = C$ and $B = 0$ also mean that $\lambda_1 = \lambda_2$, $\lambda_1^\pm = \lambda_2^\pm$, which is to say that measurements with respect to the same AP at different time points are totally independent. This is a degenerated scenario without considering temporal correlation as shown in [13]. The resulted straight-line boundaries are the same as corresponding boundaries of \mathbb{E} in [13]. This is actually corroborating our current result about the shape of boundaries.

3.2.2 Accurate Description of \mathbb{E}

Although we have a basic idea about boundaries of \mathbb{E} , it is still non-trivial to theoretically prove that the region \mathbb{E} is the same as the intuition as shown in Fig. 3-3. Imagine the detailed

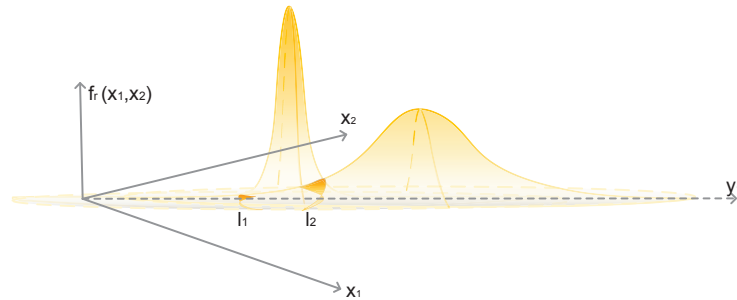


Figure 3–4: Intersection of two Gaussian PDFs.

scenario that two surfaces representing two joint Gaussian PDFs are intersecting with each other. There are actually two curves of intersection, as the two curves l_1 and l_2 illustrated in Fig. 3–4. This can be mathematically proved through simple derivation by constructing an equation between the two joint Gaussian PDFs.

It is slightly tricky to understand Fig. 3–2 and Fig. 3–4. Projections of those domes on planes $x_1-f(x_1, x_2)$ and $x_2-f(x_1, x_2)$ are the same in profile, because this is actually ignoring the temporal correlation of the RSS. Mathematically, the covariance matrix of $f_r(x_1, x_2)$ becomes variance σ^2 as the autocorrelation coefficient $\rho = 0$. However, those joint Gaussian PDFs factually have different autocorrelation coefficients denoted by ρ and ρ^\pm , as shown in Fig. 3–2; therefore, if we project those domes on the plane $y_1-f(x_1, x_2)$, the resulted image is just that illustrated in Fig. 3–4.

In the perspective of engineering, the system considers that observing fingerprints around the l_1 is with very low probability if the user is at r , thus it is more meaningful to consider the boundary represented by l_2 , in order to ensure an expected localization reliability as high as possible. It is worth mentioning that fingerprints such as those around l_1 indeed can be observed in practice. In this case, the system will estimate the location of the user is at r' , where $f_{r'}(y_1, y_2)$ has a higher value, although the user is factually at r . Such errors can not be avoided in the fingerprinting based approach, since small probability events do happen.

We can see that the opening orientation of the boundaries illustrated in Fig. 3–2 is to the left. Refer to equalities 3–9, if $\rho^- < \rho < \rho^+$, the physical meaning of the inequalities 3–9 is that: all points with the distance differences between $r - \delta$ to r and r to $r + \delta$ are less than a

constant. The opening orientation is to the left, according to the definition of the hyperbola. If $\rho^- > \rho > \rho^+$, the physical meaning of the inequalities 3–9 is that: all points with the distance differences between r to $r - \delta$ and $r + \delta$ to r are less than a constant. The opening orientation is to the right. For convenience of presentation, we here abuse the coordinate in the physical space and use the coordinate to represent the corresponding RSS values in the y_1 axis.

This means that the opening orientation of boundaries are actually determined by the degree of temporal correlation of the RSS at different locations. Moreover, no matter the relationship among ρ and ρ^\pm , the inequalities of 3–9 show that the area of \mathbb{E} is in the middle of the two boundaries. As a matter of fact, if we specifically consider the real situation under study, it should be the case $\rho^- < \rho < \rho^+$. Recall our 1-D physical model, where the AP is located at the origin of an 1-D coordinate axis and $r - \delta$, r and $r + \delta$ are distance to the AP. The farther the location is from the AP, the stronger the temporal correlation of the observed RSS will be; consequently, the orientations of the two boundaries should be to the left as shown in Fig. 3–3.

3.3 Influence of Temporal Correlation on Accuracy of Localization

We can further verify our theory by examining the expected localization result given special fingerprints. The point $(-\sqrt{2}\delta\nabla\mu, 0)$ in Fig. 4 is special, which makes $f_{r-\delta}(-\sqrt{2}\delta\nabla\mu, 0)$ to achieve the maximum value. This means that if a user reports fingerprints $(-\sqrt{2}\delta\nabla\mu, 0)$, the system definitely should estimate the user's location to be at $r - \delta$. Substituting $(-\sqrt{2}\delta\nabla\mu, 0)$ into the first inequality of (12), A natural consequence is supposed to be that the point $(-\sqrt{2}\delta\nabla\mu, 0)$ is definitely to the left of the left boundary of \mathbb{E} . However, we are surprised to find that it is possible for the point $(-\sqrt{2}\delta\nabla\mu, 0)$ to be within the region \mathbb{E} . That is, the point $(-\sqrt{2}\delta\nabla\mu, 0)$ is to the right of the left boundary of \mathbb{E} . This can happen if we set δ to be very small and the difference between ρ^- and ρ to be very large. The grey curve shown in Fig. 4 is the resulted boundary if we choose special values of δ and ρ . This event can lead to errors of location estimation, because a user definitely should be localized at $r - \delta$ is in fact localized at r .

The root cause of the phenomenon is that the choice of δ and ρ in a theoretical perspective may not comply with the real situation. In the real world, the temporal correlation in a small

neighborhood with respect to the same AP should be varying smoothly. Consequently, if δ is small, the difference between ρ^- and ρ is supposed to be insignificant.

We now compare localization results yielded by considering and ignoring the temporal correlation of the RSS. Recall the study in [13] ignores the temporal correlation of the RSS. The region \mathbb{E} in this case is the region between the two dashed lines as shown in Fig. 4. Consider shadowed areas B covered with solid lines. If the user's reported fingerprints fall into such areas, it means that the user supposed to be localized at r is mistakenly localized at $r - \delta$, or the user supposed to be localized at $r + \delta$ is mistakenly localized at r . Similarly, consider the grey areas A . If the user's reported fingerprints fall into such areas, it means that the user supposed to be localized at $r - \delta$ is mistakenly localized at r , or the user supposed to be localized at r is mistakenly localized at $r + \delta$. That is, considering temporal correlation can improve the accuracy of location estimation by providing more accurate criteria for making judgement.

Theoretically, the reliability of the localization is the probability that the user's reported fingerprints fall within the region \mathbb{E} , so that the user is localized at δ neighborhood of r . Denote the area between the two dashed lines as T . The reliability of the case where temporal correlation is now considered is

$$R(\delta, r, \sigma) = \int_T f(\mathbf{Y})d(\mathbf{Y}) = \int_{-\frac{1}{2}\delta\nabla\mu}^{\frac{1}{2}\delta\nabla\mu} f(\mathbf{Y})d(\mathbf{Y}), \quad (3-12)$$

where $f(\mathbf{Y})$ is the joint Gaussian PDF with respect to fingerprints \mathbf{Y} . Consequently, the reliability improvement by the temporal correlation is

$$\Delta R(\delta, r, \sigma, \rho) = \int_{T'-T} f(\mathbf{Y})d(\mathbf{Y}), \quad (3-13)$$

where we use T' to denote the area between the two hyperbolas.

Chapter 4 High-Dimensional Extensions for Localization

4.1 High-Dimensional Temporal Correlation

We now extend our analysis to high-dimensional temporal correlation for localization. In this case, the corresponding multivariate Gaussian distribution is with high dimension and covariance matrix Σ is with high rank. Suppose that we consider the temporal correlation of m dimension, then

$$f_r(\mathbf{x}|\mu, \Sigma) = \frac{1}{(2\pi\Sigma)^{\frac{m}{2}} |\Sigma|^{\frac{1}{2}}} e^{-\frac{1}{2}\Delta^2}, \quad (4-1)$$

where the Mahalanobis distance Δ is now as:

$$\Delta^2 = (\mathbf{x} - \mu)^T \Sigma^{-1} (\mathbf{x} - \mu). \quad (4-2)$$

Similar to the analysis procedure for the 2-dimensional temporal correlation, we can always find orthogonal eigenvectors \mathbf{u}_i using Gram Schmidt Orthogonalization (GSO) method such that

$$\Sigma = \sum_{i=1}^m \lambda_i \mathbf{u}_i \mathbf{u}_i^T, \quad \Sigma^{-1} = \sum_{i=1}^m \frac{1}{\lambda_i} \mathbf{u}_i \mathbf{u}_i^T, \quad (4-3)$$

Let $\mathbf{y} = \mathbf{U}(\mathbf{x} - \mu)$, where $\mathbf{U} = [\mathbf{u}_1, \mathbf{u}_2, \dots, \mathbf{u}_m]^T$ and $\mathbf{U}\mathbf{U}^T = \mathbf{I}$. Then the coordinate \mathbf{x} can be shifted and rotated to \mathbf{y} with Jacobian Matrix \mathbf{J} and $\mathbf{J} = \mathbf{U}^T$. The multivariate Gaussian distribution in \mathbf{y} coordinate is expressed as:

$$f_r(\mathbf{y}|\mu, \Sigma) = \frac{1}{(2\pi)^{\frac{m}{2}} (\prod_{i=1}^m \lambda_i)^{\frac{1}{2}}} e^{-\frac{1}{2} \sum_{i=1}^m \frac{1}{\lambda_i} \mathbf{y}_i \mathbf{y}_i^T}. \quad (4-4)$$

The probability of $r' \in Q$ or observation $\mathbf{x} \in E$ are the same as equation (3–6). After simplification, it is equal to

$$\begin{cases} \sum_{i=1}^m \frac{y_i^2}{\lambda_i} - \left[\frac{(y_i + \sqrt{2}\delta \nabla \mu)^2}{\lambda_i^+} + \sum_{i=2}^m \frac{y_i^2}{\lambda_i^+} \right] \leq \ln \prod_{i=1}^m \frac{\lambda_i}{\lambda_i^+}, \\ \sum_{i=1}^m \frac{y_i^2}{\lambda_i} - \left[\frac{(y_i - \sqrt{2}\delta \nabla \mu)^2}{\lambda_i^-} + \sum_{i=2}^m \frac{y_i^2}{\lambda_i^-} \right] \leq \ln \prod_{i=1}^m \frac{\lambda_i}{\lambda_i^-}. \end{cases} \quad (4-5)$$

We define vectors $\mathbf{h}_1, \mathbf{h}_2, \mathbf{h}_3$ as

$$\begin{cases} \mathbf{h}_1 = \left[\frac{y_1}{\sqrt{\lambda_1}}, \frac{y_2}{\sqrt{\lambda_2}}, \dots, \frac{y_m}{\sqrt{\lambda_m}} \right], \\ \mathbf{h}_2 = \left[\frac{y_1 + \sqrt{2}\delta \nabla \mu}{\sqrt{\lambda_1^+}}, \frac{y_2}{\sqrt{\lambda_2^+}}, \dots, \frac{y_m}{\sqrt{\lambda_m^+}} \right], \\ \mathbf{h}_3 = \left[\frac{y_1 - \sqrt{2}\delta \nabla \mu}{\sqrt{\lambda_1^-}}, \frac{y_2}{\sqrt{\lambda_2^-}}, \dots, \frac{y_m}{\sqrt{\lambda_m^-}} \right]. \end{cases} \quad (4-6)$$

The inequality sets (4–5) can be put as

$$\begin{cases} \|\mathbf{h}_1\|^2 - \|\mathbf{h}_2\|^2 \leq \sum_{i=1}^m \ln \frac{\lambda_i}{\lambda_i^+}, \\ \|\mathbf{h}_1\|^2 - \|\mathbf{h}_3\|^2 \leq \sum_{i=1}^m \ln \frac{\lambda_i}{\lambda_i^-}. \end{cases} \quad (4-7)$$

It can be seen that the boundaries of \mathbb{E} in this case is a high-dimensional hyperbola.

4.2 High-Dimensional Sample Space

Based on Maximum Likelihood Estimation (MLE), suppose the measurements for different n APs are independent and considering the temporal correlation of m dimension. Then the region \mathbb{E} should be:

$$\prod_{i=1}^n f_r(\mathbf{y}|\mu, \Sigma) \geq \prod_{i=1}^n f_{r \pm \delta}(\mathbf{y}|\mu, \Sigma). \quad (4-8)$$

Denote $y_{i,j}$ as the measurement of i th AP at the m th time points. Similar meaning to $\lambda_{i,j}$. Applying the Eq. (4-4), we have

$$\sum_{i=1}^n \sum_{j=1}^m \frac{y_{i,j}^2}{\lambda_{i,j}} - \sum_{i=1}^n \left[\frac{(y_{i,1} \pm \sqrt{2}\delta \nabla \mu_i)^2}{\lambda_{i,1}^{\pm}} \right] + \sum_{j=2}^m \frac{y_{i,j}^2}{\lambda_{i,j}^{\pm}} \leq \sum_{i=1}^n \ln \frac{|\Sigma_i|}{|\Sigma_i^{\pm}|}. \quad (4-9)$$

We here construct new vectors $\mathbf{z}_1, \mathbf{z}_2, \mathbf{z}_3$ with transformation matrix as following:

$$\mathbf{z}_1 = \begin{bmatrix} z_{11} \\ z_{12} \\ \vdots \\ z_{1m} \\ z_{21} \\ \vdots \\ z_{nm} \end{bmatrix} = \begin{bmatrix} \frac{1}{\sqrt{\lambda_{11}^+}} & 0 & \dots & 0 & 0 & \dots & 0 \\ 0 & \frac{1}{\sqrt{\lambda_{12}^+}} & \dots & 0 & 0 & \dots & 0 \\ \vdots & \vdots & \ddots & \vdots & \vdots & \ddots & \vdots \\ 0 & 0 & \dots & \frac{1}{\sqrt{\lambda_{1m}^+}} & 0 & \dots & 0 \\ 0 & 0 & \dots & 0 & \frac{1}{\sqrt{\lambda_{21}^+}} & \dots & 0 \\ \vdots & \vdots & \ddots & \vdots & \vdots & \ddots & \vdots \\ 0 & 0 & \dots & 0 & 0 & \dots & \frac{1}{\sqrt{\lambda_{nm}^+}} \end{bmatrix} \begin{bmatrix} y_{11} \\ y_{12} \\ \vdots \\ y_{1m} \\ y_{21} \\ \vdots \\ y_{nm} \end{bmatrix}. \quad (4-10)$$

and build up transformation matrix T_2 as

$$\mathbf{T}_2 = \begin{bmatrix} \frac{1}{\sqrt{\lambda_{11}^+}} & 0 & \dots & 0 & 0 & \dots & 0 & \frac{\delta \nabla \mu_1}{\sqrt{\lambda_{11}^+}} \\ 0 & \frac{1}{\sqrt{\lambda_{12}^+}} & \dots & 0 & 0 & \dots & 0 & 0 \\ \vdots & \vdots & \ddots & \vdots & \vdots & \ddots & \vdots & \vdots \\ 0 & 0 & \dots & \frac{1}{\sqrt{\lambda_{1m}^+}} & 0 & \dots & 0 & 0 \\ 0 & 0 & \dots & 0 & \frac{1}{\sqrt{\lambda_{21}^+}} & \dots & 0 & \frac{\delta \nabla \mu_2}{\sqrt{\lambda_{21}^+}} \\ \vdots & \vdots & \ddots & \vdots & \vdots & \ddots & \vdots & \vdots \\ 0 & 0 & \dots & 0 & 0 & \dots & \frac{1}{\sqrt{\lambda_{nm}^+}} & 0 \\ 0 & 0 & \dots & 0 & 0 & \dots & 0 & 1. \end{bmatrix} \quad (4-11)$$

Then the second vector \mathbf{z}_2 can be expressed as

$$\mathbf{z}_2 = \begin{bmatrix} z_{11} \\ \vdots \\ z_{nm} \\ 1 \end{bmatrix} = \mathbf{T}_2 \begin{bmatrix} y_{11} \\ \vdots \\ y_{nm} \\ 1 \end{bmatrix} \quad (4-12)$$

Similarly, define \mathbf{z}_3 to be the position $(\mathbf{r} - \vec{\delta})$ as \mathbf{z}_2 to be the position $(\mathbf{r} + \vec{\delta})$. Applying the

vectors $\mathbf{z}_1, \mathbf{z}_2, \mathbf{z}_3$ to inequality (4–9), we can get

$$\begin{cases} \|\mathbf{z}_1\|^2 - \|\mathbf{z}_2\|^2 \leq \sum_{i=1}^n \ln \frac{|\Sigma_i|}{|\Sigma_i^+|} \\ \|\mathbf{z}_1\|^2 - \|\mathbf{z}_3\|^2 \leq \sum_{i=1}^n \ln \frac{|\Sigma_i|}{|\Sigma_i^-|} \end{cases} \quad (4-13)$$

These inequations indicate that the difference of distance to two different points is a constant. By the definition of hyperbola, the boundaries of \mathbb{E} are in the shape of high-dimensional hyperbola with shearing in different dimensions.

4.3 Two-Dimensional Physical Space

We define a location in this case as a two-dimensional vector \vec{r} as shown in Fig. 1, and the joint Gaussian PDF after correlation rotation is still the multivariate Gaussian function as in Eq. (4–4). Then the probability of $\vec{r} \in Q$ or $\mathbf{x} \in \mathbb{E}$ is

$$\mathbb{E} = \left\{ \mathbf{x} \mid \prod_{i=1}^n f_{\vec{r}}(\mathbf{y} | \mu, \Sigma) \geq \prod_{i=1}^n f_{\vec{r} + \vec{\delta}}(\mathbf{y} | \mu, \Sigma) \right\}, \quad (4-14)$$

where $\vec{\delta}$ is the difference of the user's real location \vec{r} and estimated location \vec{r}' , i.e., $\vec{\delta} = \vec{r} - \vec{r}'$. We use θ to denote the angle between \vec{r} and $\vec{\delta}$ ranging from 0 to 2π , as shown in Fig. 1.

Substituting the Eq. (4–4) into Eq. (4–14), we rewrite the detailed expression of \mathbb{E} as:

$$\sum_{i=1}^n \sum_{j=1}^m \frac{y_i^2}{\lambda_{i,j}(\vec{r}')^2} - \sum_{i=1}^n \left[\frac{(y_1 + \sqrt{2}\delta \nabla \cos \theta)^2}{\lambda_{i,1}(\vec{r}')^2} + \sum_{j=2}^m \frac{y_i^2}{\lambda_{i,j}(\vec{r}')^2} \right] \leq \sum_{i=1}^n \ln \frac{|\Sigma(\vec{r}')|}{|\Sigma(\vec{r})|} \quad (4-15)$$

As the temporal correlation of the RSS is relatively stable in a small neighborhood, we can use $\nabla \rho(\vec{r})$ to denote its gradient at position \vec{r} . Refer to Fig. 2–1, a circle in the 2-D physical space is formed by rotating $\vec{\delta}$ from 0 to 2π . Consequently, the region \mathbb{E} is formed with hyperbolas in different dimensions. Intuitively, the shape of the intersection between \mathbb{E} and the corresponding orthogonal plane is irregular, because the temporal correlation in different locations can be different, which makes the curvature of the hyperbolas different from each other.

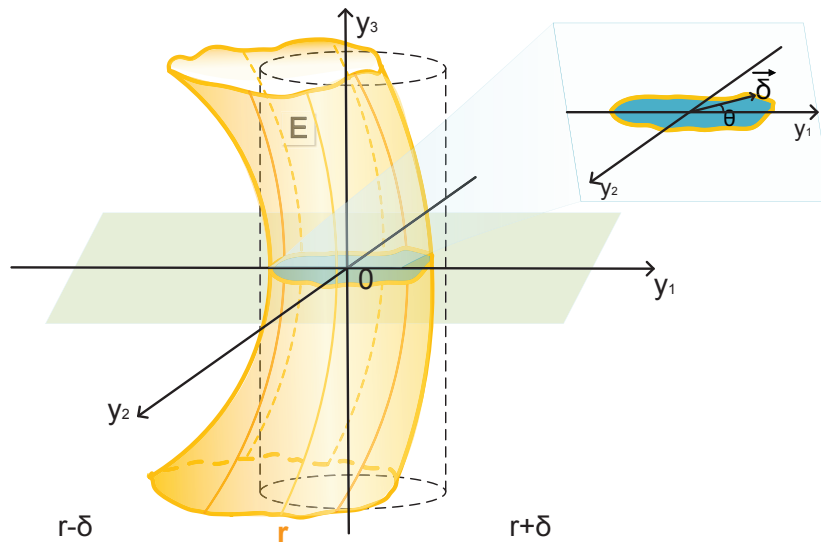


Figure 4-1: Region \mathbb{E} in 2-D physical space localization.

An abstract figure of the region \mathbb{E} in 3-D sample space and the corresponding orthogonal plane is shown as Fig. 5-1. This is because the temporal correlation in different locations can be different, which makes the curvature of the hyperbolas different from each other.

Chapter 5 Asymptotic Equivalent Region of \mathbb{E} in High-Dimensional Scenarios

This section aims to find the mathematical description of the region \mathbb{E} under the high temporal and sample dimensions and 2-D physical space. The inequality above provides a description of \mathbb{E} , which however reveals limited information about the exact shape of \mathbb{E} . This is because the inequality needs to hold for all possible values of θ and the parameter λ' is actually dependent on θ , which makes it hard to find out the shape of \mathbb{E} . Note that λ_s are actually eigenvalues of the covariance matrix $\Sigma_m(\vec{r})$, but we are unable to find the close-form expression of the eigenvalues. Our strategy to deal with the issue is to find a matrix $\Upsilon_m(\vec{r})$ to approximate $\Sigma_m(\vec{r})$, where the corresponding close-form of eigenvalues could be obtained and the resulted \mathbb{E}' is asymptotically equivalent to \mathbb{E} .

5.1 Approximate Matrix

The covariance matrix of the RSS at location \vec{r}' is

$$\Sigma_m(\vec{r}') = \begin{bmatrix} \rho_0(\vec{r}') & \rho_1(\vec{r}') & \rho_2(\vec{r}') & \cdots & \rho_{m-1}(\vec{r}') \\ \rho_1(\vec{r}') & \rho_0(\vec{r}') & \rho_1(\vec{r}') & \ddots & \rho_{m-2}(\vec{r}') \\ \rho_2(\vec{r}') & \rho_1(\vec{r}') & \ddots & \ddots & \vdots \\ \vdots & \ddots & \ddots & \ddots & \rho_1(\vec{r}') \\ \rho_{m-1}(\vec{r}') & \cdots & \rho_2(\vec{r}') & \rho_1(\vec{r}') & \rho_0(\vec{r}') \end{bmatrix}. \quad (5-1)$$

For the correlation coefficients, it is reasonable that

$$\rho_i(\vec{r}') \approx \rho_i(\vec{r}) + \nabla \rho_i(\vec{r})(\vec{r}' - \vec{r}), \quad (5-2)$$

$$\Sigma_m(\vec{r}') = \Sigma_m(\vec{r}) + \delta \cos \theta \begin{bmatrix} |\nabla \rho_0(\vec{r})| & |\nabla \rho_1(\vec{r})| & |\nabla \rho_2(\vec{r})| & \cdots & |\nabla \rho_{m-1}(\vec{r})| \\ |\nabla \rho_1(\vec{r})| & |\nabla \rho_0(\vec{r})| & |\nabla \rho_1(\vec{r})| & \ddots & |\nabla \rho_{m-2}(\vec{r})| \\ |\nabla \rho_2(\vec{r})| & |\nabla \rho_1(\vec{r})| & \ddots & \ddots & \vdots \\ \vdots & \ddots & \ddots & \ddots & |\nabla \rho_1(\vec{r})| \\ |\nabla \rho_{m-1}(\vec{r})| & \cdots & |\nabla \rho_2(\vec{r})| & |\nabla \rho_1(\vec{r})| & |\nabla \rho_0(\vec{r})| \end{bmatrix}. \quad (5-3)$$

$$\Upsilon_m(\vec{r}) = \begin{bmatrix} \rho_0(\vec{r}) & \rho_1(\vec{r}) + \rho_{m-1}(\vec{r}) & \rho_2(\vec{r}) + \rho_{m-2}(\vec{r}) & \cdots & \rho_1(\vec{r}) + \rho_{m-1}(\vec{r}) \\ \rho_1(\vec{r}) + \rho_{m-1}(\vec{r}) & \rho_0(\vec{r}) & \rho_1(\vec{r}) + \rho_{m-1}(\vec{r}) & \ddots & \rho_2(\vec{r}) + \rho_{m-2}(\vec{r}) \\ \rho_2(\vec{r}) + \rho_{m-2}(\vec{r}) & \rho_1(\vec{r}) + \rho_{m-1}(\vec{r}) & \rho_0(\vec{r}) & \ddots & \vdots \\ \vdots & \vdots & \ddots & \ddots & \rho_1(\vec{r}) + \rho_{m-1}(\vec{r}) \\ \rho_1(\vec{r}) + \rho_{m-1}(\vec{r}) & \rho_2(\vec{r}) + \rho_{m-2}(\vec{r}) & \cdots & \rho_1(\vec{r}) + \rho_{m-1}(\vec{r}) & \rho_0(\vec{r}) \end{bmatrix}. \quad (5-4)$$

because the correlation of the RSS is continuous, which has been verified in our experiments to be presented in Chapter 6. Then we have equation (5-3). We propose to use matrix $\Upsilon_m(\vec{r})$ to approximate $\Sigma_m(\vec{r})$, as shown in equation (5-4).

Suppose that the eigenvector of $\Upsilon_m(\vec{r})$ is $u = [u_1 \ u_2 \ \cdots \ u_m]$ satisfies that $\Upsilon_m(\vec{r})u = \tau(\vec{r})u$. It is easy to verify that vector $u(k) = [1, e^{i2\pi k/m}, e^{i2\pi 2k/m}, \dots, e^{i2\pi(n-1)k/n}] (1 \leq k \leq n)$ satisfies the equations and the corresponding eigenvalue is

$$\tau_{m,k}(\vec{r}) = \rho_0(\vec{r}) + \sum_{j=1}^{m-1} (\rho_j(\vec{r}) + \rho_{m-j}(\vec{r})) e^{i2\pi jk/m}. \quad (5-5)$$

We note that $\tau_{m,k}(\vec{r})$ is a real number since the coefficients of complex conjugate pairs $e^{i2\pi jk/m}$ and $e^{i2\pi j(m-k)/m}$ are identical. For the eigenvalues at location \vec{r}' , we have

$$\begin{aligned} \tau_{m,k}(\vec{r}') &= \rho_0(\vec{r}') + \sum_{j=1}^{m-1} (\rho_j(\vec{r}') + \rho_{m-j}(\vec{r}')) e^{i2\pi jk/m} \\ &= \tau_{m,k}(\vec{r}) + \delta \cos \theta \sum_{j=1}^{m-1} (|\nabla \rho_j(\vec{r})| + |\nabla \rho_{m-j}(\vec{r})|) e^{i2\pi kj/m}. \end{aligned} \quad (5-6)$$

To simplify the notations, we use $\Delta\tau_{m,k}$ to represent $\sum_{j=1}^{m-1} (|\nabla \rho_j(\vec{r})| + |\nabla \rho_{m-j}(\vec{r})|) e^{i2\pi kj/m}$, thus $\tau_{m,k}(\vec{r}') = \tau_{m,k}(\vec{r}) + \delta \cos \theta \Delta\tau_{m,k}$.

We are to prove that using $\tau_{m,k}(\vec{r})$ to approximate eigenvalues of $\Sigma_m(\vec{r})$ could incur the error converging to zero as m goes to infinity.

5.2 Asymptotical Equivalence Analysis

We take another form of region \mathbb{E} as following to facilitate understanding:

$$\sum_{i=1}^m \frac{y_i^2}{\lambda_{m,i}(\vec{r})} - \left[\frac{(y_1 + \sqrt{2}\delta\nabla \cos \theta)^2}{\lambda_{m,1}(\vec{r}')^2} + \sum_{i=1}^m \frac{y_i^2}{\lambda_{m,i}(\vec{r}')^2} \right] \leq \ln \frac{|\Sigma(\vec{r})|}{|\Sigma(\vec{r}')|}, \quad (5-7)$$

where $\theta \in [0, \pi]$. If we use eigenvalues of matrix $\Upsilon_m(\vec{r})$ to replace $\lambda_i(\vec{r}')$, we could obtain the region \mathbb{E}' characterized by the following equation:

$$\sum_{i=1}^m \frac{y_i^2}{\tau_{n,i}(\vec{r})} - \left[\frac{(y_1 + \sqrt{2}\delta\nabla \cos \theta)^2}{\tau_{m,1}(\vec{r}')^2} + \sum_{i=1}^m \frac{y_i^2}{\tau_{m,i}(\vec{r}')^2} \right] \leq \ln \frac{|\Upsilon_m(\vec{r})|}{|\Upsilon_m(\vec{r}')|}. \quad (5-8)$$

Lemma 1. $\lim_{m \rightarrow \infty} |\Upsilon_m(\vec{r}) - \Sigma(\vec{r})|^2 = 0$, where $|\cdot|^2$ represents the Hilbert-Schmidt Norm.

Proof.

$$\Upsilon_m(\vec{r}) - \Sigma(\vec{r}) = \begin{bmatrix} 0 & \rho_{m-1}(\vec{r}) & \rho_{m-2}(\vec{r}) & \cdots & \rho_1(\vec{r}) \\ \rho_{m-1}(\vec{r}) & 0 & \rho_{m-1}(\vec{r}) & \ddots & \rho_2(\vec{r}) \\ \rho_{m-2}(\vec{r}) & \rho_{m-1}(\vec{r}) & 0 & \ddots & \vdots \\ \vdots & & \ddots & \ddots & \rho_{m-1}(\vec{r}) \\ \rho_1(\vec{r}) & \rho_2(\vec{r}) & \cdots & \rho_{m-1}(\vec{r}) & 0 \end{bmatrix}. \quad (5-9)$$

With the definition of *Hilbert-Schmidt Norm*,

$$|\Sigma(\vec{r}) - \Upsilon_n(\vec{r})|^2 = 2 \sum_{i=1}^{n-1} \frac{i}{n} \rho_i^2(\vec{r}), \quad (5-10)$$

we will show that

$$\lim_{m \rightarrow \infty} \sum_{i=1}^{m-1} \frac{i}{m} \rho_i^2(\vec{r}) = 0. \quad (5-11)$$

By applying *Abel Transformation* to the equation above, we obtain that

$$\sum_{i=1}^{m-1} \frac{i}{m} \rho_i^2(\vec{r}) = \frac{m-1}{m} A_{m-1} - \sum_{i=1}^{m-2} \frac{1}{m} A_i, \quad (5-12)$$

where $A_i = \sum_{j=1}^i \rho_j^2(\vec{r})$. Since the covariances are absolutely summable with $\sum_i \rho_i < \infty$, we use A to denote the supremum of $\sum \rho_j^2(\vec{r})$, i.e., $A = \sup \sum \rho_j^2(\vec{r})$. Consequently, we can find N such that $A > A_k > A - \varepsilon$ holds for all the $k \geq N$ for any $\varepsilon > 0$. Hence

$$A > \sum_{i=1}^{m-2} \frac{1}{m} A_i = \frac{1}{m} \left(\sum_{i=1}^{N-1} A_i + \sum_{i=N}^{m-2} A_i \right) > \frac{m-N-1}{m} (A - \varepsilon). \quad (5-13)$$

Notice that

$$\lim_{m \rightarrow \infty} \frac{m-N-1}{m} (A - \varepsilon) = A - \varepsilon \quad (5-14)$$

, we thus have proven that for any $\varepsilon > 0$, $\lim_{m \rightarrow \infty} \sum_{i=1}^{m-2} \frac{1}{m} A_i > A - \varepsilon$.

Combined with the fact that $\sum_{i=1}^{m-2} \frac{1}{m} A_i < A$, we can conclude that

$$\lim_{m \rightarrow \infty} \sum_{i=1}^{m-2} \frac{1}{m} A_i = A = \lim_{n \rightarrow \infty} \frac{m-1}{m} A_{m-1}. \quad (5-15)$$

The proof is completed. □

Lemma 2. (*Wielandt-Hoffman theorem [37]*) Given two Hermitian matrices A and B with eigenvalues α_k and β_k respectively, then

$$\frac{1}{m} \sum_{i=1}^m |\alpha_k - \beta_k|^2 \leq |A - B|^2. \quad (5-16)$$

We present the lemma for the purpose of self-completeness.

Lemma 3. For any given integer s , we have

$$\lim_{m \rightarrow \infty} \frac{1}{m} \sum_{i=1}^m (\tau_{m,k}^s(\vec{r}) - \lambda_{m,k}^s(\vec{r})) = 0. \quad (5-17)$$

Proof. Note that

$$\begin{aligned} & \frac{1}{m} \sum_{i=0}^{s-1} \left| \tau_{m,k}^s(\vec{r}) - \lambda_{m,k}^s(\vec{r}) \right| \\ & \frac{1}{m} \sum_{i=0}^{s-1} |\tau_{m,k}(\vec{r}) - \lambda_{m,k}(\vec{r})| \left| \sum_{i=0}^{s-1} \tau_{m,k}^i(\vec{r}) \lambda_{m,k}^{s-i-1}(\vec{r}) \right| \\ & \leq \frac{sM^{s-1}}{n} \sum_{i=0}^{s-1} |\tau_{m,k}(\vec{r}) - \lambda_{m,k}(\vec{r})| \\ & \leq sM^{s-1} \sqrt{\frac{1}{m} \sum_{i=1}^m |\tau_{m,k}(\vec{r}) - \lambda_{m,k}(\vec{r})|^2} \\ & \leq sM^{s-1} |A - B|, \end{aligned} \quad (5-18)$$

where s and M are constants with respect to m . The penult inequality is based on Cauchy-Schwarz Inequality and the last inequality is based on Lemma 2. Then the proof is completed. \square

With *Weierstrass' theorem*, we know that there exists a sequence of polynomials $[P_t(x)]$ such that $\lim_{t \rightarrow \infty} P_t(x) = \frac{1}{x}$. For every fixed t , we know that

$$\lim_{m \rightarrow \infty} \frac{1}{m} \sum_{i=1}^m |P_t(\tau_{m,i}(\vec{r})) - P_t(\lambda_{m,i}(\vec{r}))| = 0 \quad (5-19)$$

according to Lemma 3. Hence combining the two equations above, we can obtain that

$$\lim_{m \rightarrow \infty} \frac{1}{m} \sum_{i=1}^m \left| \frac{1}{\tau_{m,i}} - \frac{1}{\lambda_{m,i}} \right| = 0. \quad (5-20)$$

Theorem 1. *The region \mathbb{E}' is asymptotical equivalent to region \mathbb{E} , that is to say:*

$$\begin{aligned}
 (1) : \lim_{m \rightarrow \infty} \frac{1}{m} \left\{ \sum_{i=1}^m \left[\frac{y_i^2}{\lambda_{m,i}(\vec{r})} - \frac{y_i^2}{\tau_{m,i}(\vec{r})} \right] - \sum_{i=1}^m \left[\frac{y_i^2}{\lambda_{m,i}(\vec{r}')} - \frac{y_i^2}{\tau_{m,i}(\vec{r}')} \right] \right. \\
 \left. - \left[\frac{(y_1 + \sqrt{2}\delta\nabla \cos \theta)^2}{\lambda_{m,1}(\vec{r})} - \frac{(y_1 + \sqrt{2}\delta\nabla \cos \theta)^2}{\tau_{m,1}(\vec{r})} \right] \right\} = 0; \quad (5-21) \\
 (2) : \lim_{m \rightarrow \infty} \left\{ \ln \frac{|\Sigma(\vec{r})|^{\frac{1}{m}}}{|\Sigma(\vec{r}')|^{\frac{1}{m}}} - \ln \frac{|\Upsilon_m(\vec{r})|^{\frac{1}{m}}}{|\Upsilon_m(\vec{r}')|^{\frac{1}{m}}} \right\} = 0.
 \end{aligned}$$

Proof. The RSS can be observed at each location is bounded, hence y_i^2 s and $(y_1 + \sqrt{2}\delta\nabla \cos \theta)^2$ are bounded. Suppose that their upper bound is M , then

$$\frac{1}{m} \left| \begin{aligned} & \sum_{i=1}^m \left[\frac{y_i^2}{\lambda_{m,i}(\vec{r})} - \frac{y_i^2}{\tau_{m,i}(\vec{r})} \right] - \sum_{i=2}^m \left[\frac{y_i^2}{\lambda_{m,i}(\vec{r}')} - \frac{y_i^2}{\tau_{m,i}(\vec{r}')} \right] \\ & - \left[\frac{(y_1 + \sqrt{2}\delta\nabla \cos \theta)^2}{\lambda_{m,1}(\vec{r})} - \frac{(y_1 + \sqrt{2}\delta\nabla \cos \theta)^2}{\tau_{m,1}(\vec{r})} \right] \end{aligned} \right| \leq \frac{2M}{m} \sum_{i=1}^m \left| \frac{1}{\tau_{m,k}(\vec{r})} - \frac{1}{\lambda_{m,k}(\vec{r})} \right|. \quad (5-22)$$

Combined with Eq. 6–4, we know that the first part of theorem holds. The proof of the second part is similar. By using *Weierstrass' theorem*, we know that there exists a sequence of polynomials $Q_t(\tau_{m,k}(\vec{r}))$ such that $\lim_{t \rightarrow \infty} P_t(\tau_{m,k}(\vec{r})) = \ln \tau_{m,k}(\vec{r})$. Combined with Lemma 3, we have

$$\lim_{m \rightarrow \infty} \frac{1}{m} \sum_{i=1}^m |\ln \tau_{m,k}(\vec{r}) - \ln \lambda_{m,k}(\vec{r})| = 0 \quad (5-23)$$

Notice that

$$\frac{1}{m} \sum_{i=1}^m |\ln \tau_{m,k}(\vec{r}) - \ln \lambda_{m,k}(\vec{r})| \geq \frac{1}{m} \left| \ln \frac{|\Sigma(\vec{r})|^{\frac{1}{m}}}{|\Upsilon_m(\vec{r})|^{\frac{1}{m}}} \right|, \quad (5-24)$$

which means that

$$\lim_{m \rightarrow \infty} \frac{1}{m} \left| \ln |\Sigma(\vec{r})|^{\frac{1}{m}} - \ln |\Upsilon_m(\vec{r})|^{\frac{1}{m}} \right| = 0. \quad (5-25)$$

With the same virtue,

$$\lim_{m \rightarrow \infty} \frac{1}{m} \left| \ln |\Sigma(\vec{r}')|^{\frac{1}{m}} - \ln |\Upsilon_m(\vec{r}')|^{\frac{1}{m}} \right| = 0. \quad (5-26)$$

Combining these two equations, the second part of this theorem is proved. \square

5.3 Boundaries of Region \mathbb{E}'

We define the *Fourier Transformation* of the covariance series as:

$$g(\omega, \vec{r}) = \sum_{j=-\infty}^{\infty} \rho_j(\vec{r}) e^{i2\pi\omega j}, \quad -\frac{1}{2} < \omega \leq \frac{1}{2}. \quad (5-27)$$

According to *Szego's theorem* [sze], for an arbitrary continuous function G , we have

$$\lim_{m \rightarrow \infty} \frac{1}{m} \sum_{k=0}^{m-1} G(\tau_{m,k}(\vec{r})) = \int_{-1/2}^{1/2} G(g(\omega), \vec{r}) d\omega. \quad (5-28)$$

Let $G(x) = \ln x$, we can obtain the approximate expression of the determinant of Σ_m :

$$\ln |\Sigma_m(\vec{r})|^{1/m} = \frac{1}{m} \sum \ln \tau_{m,k}(\vec{r}) \approx \int_{-1/2}^{1/2} \ln g(\omega, \vec{r}) d\omega. \quad (5-29)$$

For the matrix $\Sigma_m(\vec{r}')$, the corresponding Fourier Transformation is

$$g(\omega, \vec{r}') = \sum_{j=-\infty}^{\infty} \rho_j(\vec{r}') e^{i2\pi\omega j} = g(\omega, \vec{r}) + \delta \cos \theta \sum_{j=-\infty}^{\infty} |\nabla \rho_j(\vec{r})| e^{i2\pi\omega j}, \quad -\frac{1}{2} < \omega \leq \frac{1}{2}. \quad (5-30)$$

Similarly, we can use

$$m \int_{-1/2}^{1/2} \ln [g(\omega, \vec{r}') + \delta \cos \theta \sum_{j=-\infty}^{\infty} |\nabla \rho_j(\vec{r})| e^{i2\pi\omega j}] d\omega \quad (5-31)$$

to estimate the term $\ln |\Sigma_m(\vec{r}')|$.

Notice that

$$\partial \frac{\ln \frac{|\Sigma_m(\vec{r}')|^{1/m}}{|\Sigma_m(\vec{r})|^{1/m}}}{\partial \theta} = \frac{\delta \sin \theta \sum_{j=-\infty}^{\infty} |\nabla \rho_j(\vec{r})| e^{i2\pi\omega j}}{g(\omega, \vec{r}) + \delta \cos \theta \sum_{j=-\infty}^{\infty} |\nabla \rho_j(\vec{r})| e^{i2\pi\omega j}} = O(\delta \sin \theta). \quad (5-32)$$

Since δ is a bounded real number and $|\sin \theta| \leq 1$,

$$\frac{d \ln \frac{|\Sigma_m(\vec{r})|^{\frac{1}{m}}}{|\Sigma_m(\vec{r}')|^{\frac{1}{m}}}}{d\theta} \approx 0. \quad (5-33)$$

Moreover, $\partial \frac{[(y_1 + \sqrt{2}\delta\nabla \cos \theta)^2 + \sum_{i=1}^m \frac{y_i^2}{\lambda_i(\vec{r}')}]^{\frac{1}{2}}}{\partial \theta} = \sin \theta [h(\cos \theta) - c]$, where $h(\cdot)$ is a monotone function with respect to $\cos \theta$ and c is a positive number. Note that $\theta \in [0, \pi]$, thus there is at most one root of function $\sin \theta [h(\cos \theta) - c]$ in $[0, \pi]$. We use θ^* to denote this root; therefore, the minimum value of function $\frac{(y_1 + \sqrt{2}\delta\nabla \cos \theta)^2}{\lambda_i(\vec{r}')} + \sum_{i=1}^n \frac{y_i^2}{\lambda_i(\vec{r}')}$ is achieved under these three cases:

$$\begin{cases} \cos \theta = -1, \\ \cos \theta = 1, \\ \cos \theta = \cos \theta^*. \end{cases} \quad (5-34)$$

Consequently, the boundaries of the region \mathbb{E}' can be described by the following three hypersurfaces:

$$F_1 : \sum_{t=1}^n \frac{y_i^2}{\tau_{n,t}(\vec{r})} - \left[\frac{(y_1 - \sqrt{2}\delta\nabla)^2}{\tau_{n,1}(\vec{r}) - \delta\Delta\tau_{n,1}} + \sum_{t=2}^n \frac{y_i^2}{\tau_{n,t}(\vec{r}) - \delta\Delta\tau_{n,t}} \right] \leq \ln \frac{|\Sigma(\vec{r})|}{|\Sigma(\vec{r}')|} \quad (5-35)$$

$$F_2 : \sum_{t=1}^n \frac{y_i^2}{\tau_{n,t}(\vec{r})} - \left[\frac{(y_1 + \sqrt{2}\delta\nabla)^2}{\tau_{n,1}(\vec{r}) + \delta\Delta\tau_{n,1}} + \sum_{t=2}^n \frac{y_i^2}{\tau_{n,t}(\vec{r}) + \delta\Delta\tau_{n,t}} \right] \leq \ln \frac{|\Sigma(\vec{r})|}{|\Sigma(\vec{r}')|} \quad (5-36)$$

$$F_3 : \sum_{t=1}^n \frac{y_i^2}{\tau_{n,t}(\vec{r})} - \left[\frac{(y_1 + \sqrt{2}\delta \cos \theta^* \nabla)^2}{\tau_{n,1}(\vec{r}) + \delta \cos \theta^* \Delta\tau_{n,1}} + \sum_{t=2}^n \frac{y_i^2}{\tau_{n,t}(\vec{r}) + \delta \cos \theta^* \Delta\tau_{n,t}} \right] \leq \ln \frac{|\Sigma(\vec{r})|}{|\Sigma(\vec{r}')|} \quad (5-37)$$

The results above is for the single measurement case, which means that only one observed RSS reading is submitted to the server for location estimation.

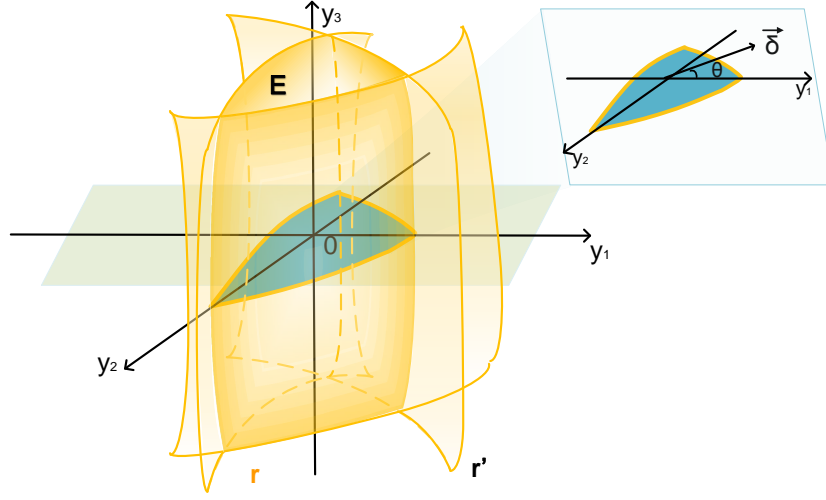


Figure 5-1: Simplified Region \mathbb{E} with high dimensional samplings in 2-D physical space.

The results can be further extended to the case where the user could report RSS readings from n independent APs. The corresponding region \mathbb{E} should be:

$$\sum_{i=1}^n \left[\sum_{j=1}^m \frac{y_{i,j}^2}{\lambda_{i,j}(\vec{r})} - \sum_{i=1}^n \left[\frac{(y_{i,1} + \sqrt{2}\nabla \cos \theta)^2}{\lambda_{i,1}(\vec{r}')} + \sum_{j=2}^m \frac{y_{i,j}^2}{\lambda_{i,j}(\vec{r}')} \right] \right] \leq \sum_{i=1}^n \ln \frac{|\Sigma_i(\vec{r})|}{|\Sigma_i(\vec{r}')|}. \quad (5-38)$$

Note that there are n items in the outlayer sum sequence and the i th item

$$\sum_{j=1}^m \frac{y_{i,j}^2}{\lambda_{i,j}(\vec{r})} - \sum_{i=1}^n \left[\frac{(y_{i,1} + \sqrt{2}\nabla \cos \theta)^2}{\lambda_{i,1}(\vec{r}')} + \sum_{j=2}^m \frac{y_{i,j}^2}{\lambda_{i,j}(\vec{r}')} \right] \leq \ln \frac{|\Sigma_i(\vec{r})|}{|\Sigma_i(\vec{r}')|} \quad (5-39)$$

corresponds to the i th measurement. We can use the techniques in the single measurement scenario to figure out the approximation region \mathbb{E}' .

Chapter 6 Location Estimation Facilitated by Temporal Correlation of the RSS

After revealing the fundamental reason why accuracy of location estimation could be improved by taking temporal correlation of the RSS into account, this section presents how to utilize the theoretical results above in practical localization process. In this section, we demonstrate the evaluation and experimental results to show the performance differences between the system utilizing and the system ignoring temporal correlation of the RSS.

6.1 Feasibility of Utilizing Temporal Correlation

We first investigate whether location estimation could be facilitated with the information of temporal correlation in practice. The experiments are conducted in a laboratory indoor environment to verify our analysis for the 2-D physical space. We conduct experiments in an square indoor space that is a around $40m^2$. The square is divided into grids with the edge length of $60cm$. We use six mobile devices to measure the RSSes from all APs detected at 110 ($11*10$) different locations. We measure the RSS value every 25 millisecond for 4k times at each location. Traditional localization estimation processes extract the RSS information independently and build the corresponding PDF in the database, such as the mean value of RSS distribution shown in Fig. 6–1 (b).

We illustrate the spatial distribution of ρ in Fig. 6–1 (a), where the values of ρ in different locations are derived from the locally sampled RSSes. The method for deriving those values are to be described in the following subsection. We randomly select an pre-existing AP and measure its RSS. It is interesting to find that the values of ρ are basically increasing as the distance between the sampling location and the AP's location is increasing, while the values of μ are basically decreasing, as shown in Fig. 6–1 (b). That is the nearer the location is to the AP,

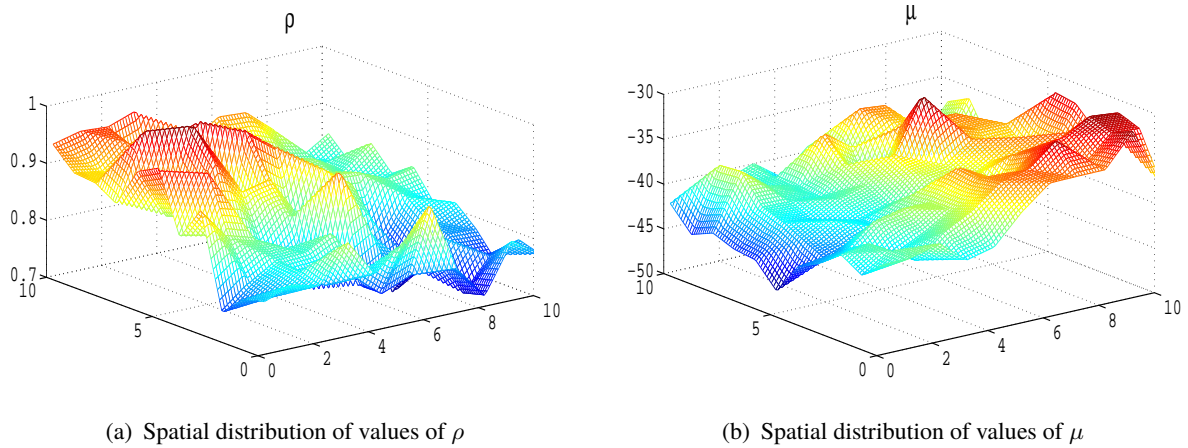


Figure 6–1: Spatial distribution of values of ρ and μ

the signal strength is stronger and the mean values of the RSS are higher; the farther the location is to the AP, the signal strength is vanishing thus the sequentially observed RSSes are basically the same. The temporal correlation trends to be enhanced when the distance is larger. This is because the region of vibration is limited when the RSS value are small at a far place. When at a place close to the AP, its signal strength has more liberty at the near place. In other words, the vibrations of signal are allayed by the fading, shadowing or multi-path effects.

Figure 6–2 associates the values of μ and ρ with locations, where the horizontal axis represents the indices of locations. We sort the locations according to the locally sampled values of μ , and the corresponding values of ρ are also plotted. In this way, we want to verify whether the temporal correlation information is useful by comparing it to the previous measures, i.e. mean and sigma. If the temporal correlation has a distinct relation with the positions, we can say it is an additional information to the previous method, which means we can double the useful metrics without inflating the training database.

As we can see from Fig. 6–2, the values of ρ present distinct pattern compared with μ in different locations. The situation of σ and ρ is similar to that of μ . When sorted the values of means with positions marked on them, the ρ has little coherence with the mean and sigma, which means the potential ability of temporal correlation information to facilitate the useful database for localization. In fact, we calculate the cross correlation between μ , σ and ρ , whose values are around -0.5 which indicates that the values are not definitely related to each other.

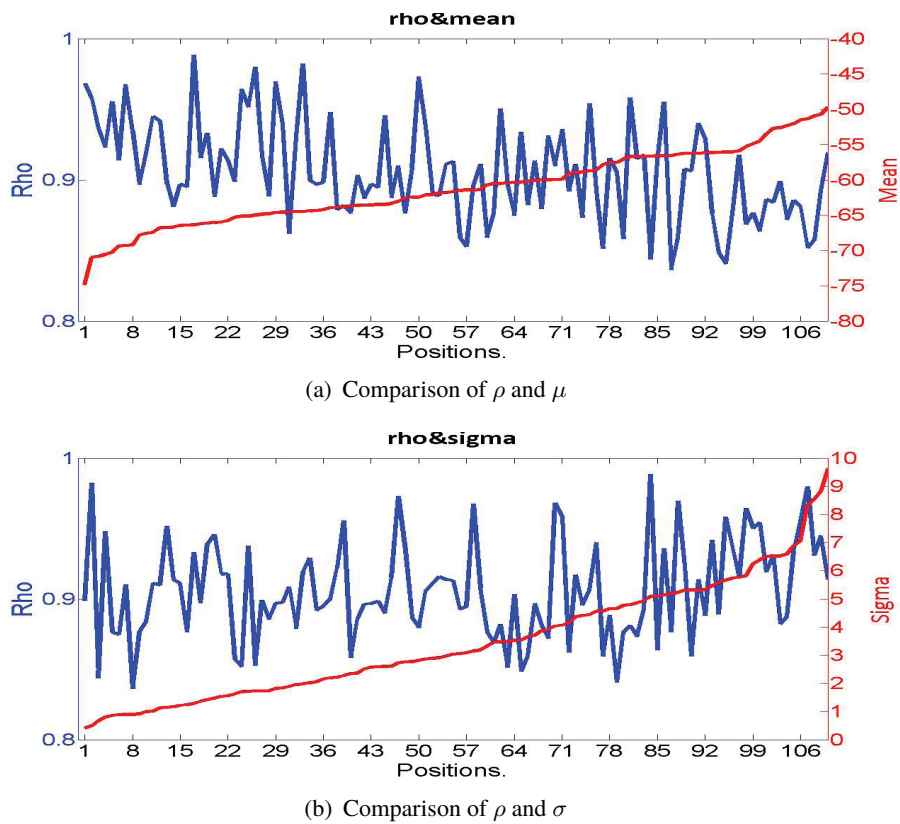


Figure 6–2: Comparison of Correlation ρ , Variance σ and Mean Value

The experiment results illustrated above indicate that the temporal correlation information of the RSS provides a diversified feature compared with the information of μ , σ and ρ . The temporal correlation could be used to cross check the result of location estimation. It is worth mentioning that the values of ρ can be derived from the sampled RSSes thus incur no extra overhead in the training phase.

Through our investigation, we found it is rarely fully studied on the temporal correlation of Wi-Fi signal strength. Since temporal correlation of RSS makes big differences in localization systems, in next part, we would make a thorough analysis of the properties of the correlation coefficient and design an algorithm to show what we should do to utilize such information.

6.2 Localization Estimation Algorithm

Suppose that we sample w RSSes from AP_i , then we could construct an intermediate matrix A before computing the covariance matrix $\Sigma_i(\vec{r})$:

$$A = \begin{bmatrix} x_{i,1} & x_{i,2} & \cdots & x_{i,m-1} & x_{i,m} \\ x_{i,2} & x_{i,3} & \cdots & x_{i,m} & x_{i,m+1} \\ \vdots & \vdots & \ddots & \vdots & \vdots \\ x_{i,w-m} & x_{i,w-m+1} & \cdots & x_{i,w-2} & x_{i,w-1} \\ x_{i,w-m+1} & x_{i,w-m+2} & \cdots & x_{i,w-1} & x_{i,w} \end{bmatrix} \quad (6-1)$$

where we assume that only m -dimensional temporal correlation is considered. The second subscript of each entry of the matrix means the j th measurement with respect to AP_i . It is easy to find that the mean value μ_k of each vector A_k^T is

$$\mu_k = \frac{\sum_{j=k}^{w-m+k} x_{i,j}}{w - m + 1}. \quad (6-2)$$

With *Maximum Likelihood Estimation (MLE)*, we estimate the correlation matrix as

$$\Sigma_{k,j}(\vec{r}) = Cov[A_k^T, A_j^T] = \frac{(A_k^T - \mu_k)^T (A_j^T - \mu_j)}{\sigma^2(w - m + 1)}, \quad (6-3)$$

where k and j equals to $1, 2, \dots, m$, respectively.

Equation (6-3) is equivalent to the following equation:

$$\Sigma_{k,j}(\vec{r}) = \frac{\sum_{t=0}^{w-m} (x_{i,k+t} - \mu_k)(x_{i,j+t} - \mu_j)}{\sigma^2(w - m + 1)} = \frac{\sum_{t=0}^{w-m} x_{i,k+t}x_{i,j+t}}{\sigma^2(w - m + 1)} - \frac{\mu_k\mu_j}{\sigma^2}; \quad (6-4)$$

therefore

$$\Sigma_{k+1,j+1}(\vec{r}) - \Sigma_{k,j}(\vec{r}) = \frac{x_{i,j+w-m+1}x_{i,k+w-m+1} - x_{i,j}x_{i,k}}{\sigma^2(w - m + 1)} + \frac{\mu_k\mu_j - \mu_{k+1}\mu_{j+1}}{\sigma^2}. \quad (6-5)$$

Notice that

$$\mu_k - \mu_{k+1} = \frac{x_{i,k} - x_{i,k+w-m+1}}{w - m + 1} = O\left(\frac{1}{w - m + 1}\right) \quad (6-6)$$

and

$$\left[\frac{\mu_k \mu_j - \mu_{k+1} \mu_{j+1}}{\sigma^2} = \frac{\mu_j}{\sigma^2} (\mu_k - \mu_{k+1}) + \frac{\mu_{k+1}}{\sigma^2} (\mu_j - \mu_{j+1}) \right], \quad (6-7)$$

and $\Sigma_{k+1,j+1}(\vec{r}') - \Sigma_{k,j}(\vec{r}') = O\left(\frac{1}{w-m+1}\right)$. To better estimate the parameters, often the number of samples m should be large enough, which indicates that $\Sigma_{k+1,j+1}(\vec{r}') - \Sigma_{k,j}(\vec{r}')$ is very small, so it is reasonable to assume that the covariance matrix is in the form

$$\Sigma = \sigma^2 \begin{bmatrix} 1 & \rho_2 & \cdots & \rho_{m-1} & \rho_m \\ \rho_2 & 1 & \cdots & \rho_{m-2} & \rho_{m-1} \\ \vdots & \vdots & \ddots & \vdots & \vdots \\ \rho_{m-1} & \rho_{m-2} & \cdots & 1 & \rho_2 \\ \rho_m & \rho_{m-1} & \cdots & \rho_2 & 1. \end{bmatrix} \quad (6-8)$$

Algorithm 6-1 illustrates how to utilize temporal correlation for better location estimation, which is in essence a synthetic approach integrating the information of both the mean value and the temporal correlation of the RSS.

Algorithm 6-1 Temporal Correlation for Location Estimation

Input parameters:

The training data set for each location \vec{r} , x_{ij} ($i = 1 \dots n$; $j = 1 \dots w$);

The reported RSS sequence t_{ij} ($i = 1 \dots a$; $j = 1 \dots b$) from a user;

Indoor space L is a set of all the identified locations recorded in the database;

Threshold Th is the critical value of choice for mean vectors.

1. For each location i in L , calculate the mean vector $\mu_i = (\mu_1, \mu_2, \dots, \mu_m)$ with equation 6-2, and calculate the correlation vector $\rho_i = (\rho_1, \rho_2, \dots, \rho_m)$ as equation 6-3 shows.
 2. For the reported data t_{ij} from a user, also calculate the target mean and correlation vectors as μ_t, ρ_t .
 3. Find the Euclidean distance between μ_t and every μ_i . Find all the vectors μ_k among those μ_i s, and the distance between each μ_k and μ_t should be within Th in the sample space, i.e., $|\mu_i - \mu_t| \leq Th$. The corresponding locations associated with those μ_k s are denoted using a set $\{\mathbf{l}_{kmin}\}$.
 4. Compare the Euclidean distance between ρ_t and ρ_i in $\{\mathbf{l}_{kmin}\}$. Find the vector that is nearest to ρ_t . The nearest distance in correlation sample space is the place we localize the user at.
-

The basic idea of the algorithm is that we first find a list of candidate locations of the user with the mean value comparison as most of the work in the literature does, and then find the most likely location with the temporal correlation comparison.

6.3 Choice of Design Parameters

Design parameters must be chosen before the algorithm presented above can be appropriately utilized. In order to make good use of the temporal correlation information and reduce the complexity of training process, we need to find the most appropriate value of parameters like the dimension of ρ , the time interval as well as the number of training set. We conduct experiments to show how to choose the number of temporal dimension, the sampling interval and number of samplings in practice. These factors influence the value of ρ in a location, and a distinguishable value of ρ in a location is favored in the localization process.

We calculate the temporal correlation coefficient ρ from 2-dimension to 280-dimension. The results are shown in Fig. 6–3. Interestingly we found that at the beginning with dimensions

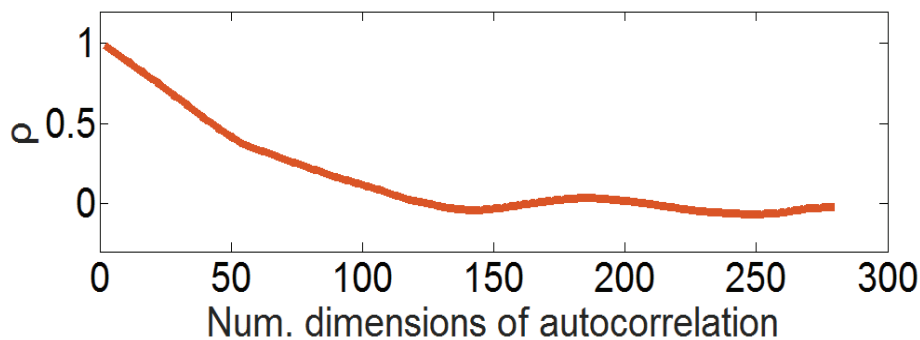


Figure 6–3: Parameter analysis of the number of correlation dimensions

smaller than 50, it shows as a linearly attenuation of correlation. When continued to increase the dimension, the descent ratio becomes smaller. And on the higher dimensions, it shows nearly no correlation as it changes around zero. We can find that the value of ρ decreases as the number of dimensions increases and then keeps comparatively flat. The value of ρ is at around 0 when the number of dimensions goes beyond 100, which indicates that it is meaningless to consider over-high dimensions. The current value of RSS becomes almost irrelevant compared with the

values of RSS sampled long time ago. We can also find that the number of dimensions 50 is a critical point, after which the trend of ρ becomes flat. Consequently, we recommend to utilize the information of the temporal correlation with the number of dimensions that are less than 50 in practice.

The effectiveness of the temporal correlation also depends on the length of the interval that sequential RSS samplings are performed. Figure 6–4 shows the corresponding values of ρ under different sampling intervals varying from $25ms$ to $200ms$. It shows like a linearly

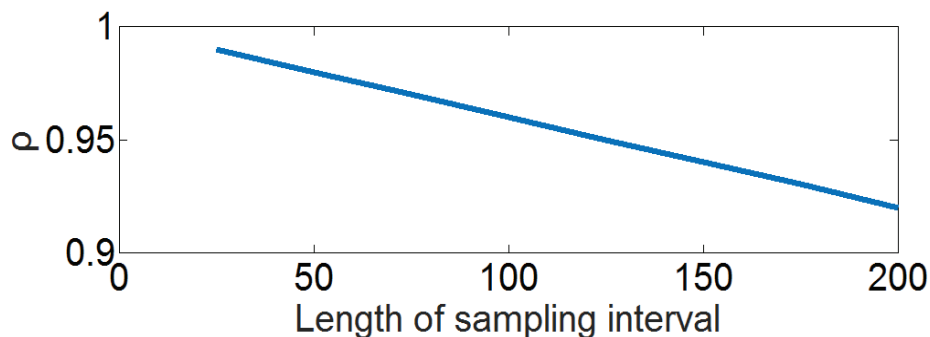


Figure 6–4: Parameter analysis of the sampling interval

descending when the interval increases. It is straightforward that the values of ρ are decreasing as the length of the interval increases, because the longer the interval is the more unrelated the currently sampled RSS values are from the previous ones. On the one hand, we cannot use the smallest time intervals as the RSS values are repeated for almost several dozen times, which cause great redundancy. So over-short sampling interval is unnecessary, since the RSS readings may not change that fast and the observed values of the RSS are basically the same in this case. On the other hand, the large time intervals are also not suitable, as the temporal correlation is attenuated too much that may result in the deterioration of its quality. Overall, it is appropriate to set a medial τ . In this case, we choose $100ms$ as the length of sampling interval, which is proved to be appropriate in the experiments to be presented later.

After the number of dimensions and the sampling interval are determined, we still need to decide the starting point of the sampling. This is because we could see variance of ρ at the first amount of sampling intervals, as shown in Figure 6–5. We need to retrieve those RSSes that could yields comparatively stable temporal correlation information. To this end, we sample

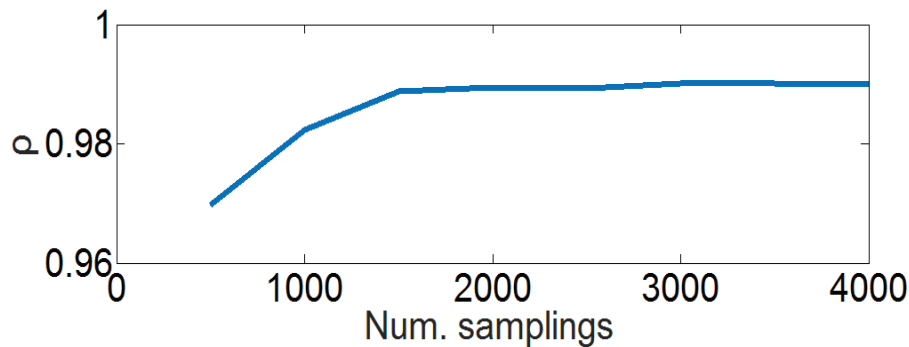


Figure 6–5: Parameter analysis of the number of samplings

2000 RSS values in our system, since the value of ρ tends to be stable after the 1500th sampling as shown in this figure.

In order to further present the stability of temporal correlation, we compare the correlation efficient of Access Point "CMCC-EDU" with different number of samplings. As shown in Fig. 6–6, the horizontal axis is the id of reference points; the vertical axis is the temporal correlation coefficient; the blue line is calculated with 1500 RSS samplings, and the red line is calculated by 4000 RSSes. We can see that most points stays consistent with each other at

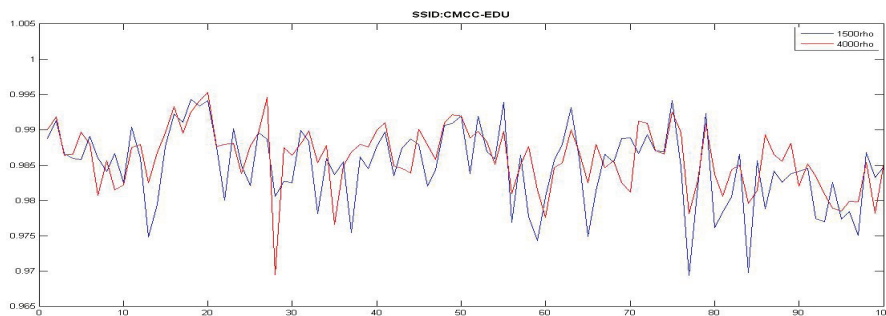


Figure 6–6: Comparison of correlation with different sampling number

each reference point, so these two correlation values with different sampling number can be a reference as position information.

In this chapter, we do control experiments to elaborate the feasibility of the temporal correlation information in localization system, and find the proper choice of key design parameters. Combined with all the reasonable discovery in experiment, we design an algorithm for fingerprinting indoor localization utilizing temporal correlation coefficients.

Chapter 7 Simulation and Experiment Results

In this chapter, we will integrate all the previous theoretical analysis and algorithm design in a real positioning system and show our improvements. First section would be the introduction and details of system setups and implementation. Next part is a model-based trace-driven simulation, which is totally for the interest of proving the aforementioned theoretical analysis. The last section is the experimental result in reliability improvement.

7.1 System Setups

We built a localization system prototype to show the advantage of leveraging temporal correlation of signal strength. The whole procedure of fingerprinting localization system could be described as this: First, in the experimental indoor area, we divide the region in grids as reference points with required accuracy as radius. And then, detect the n visible wireless access points naturally deployed before without knowing locations. After that, collect the RSS fingerprint for w time for each AP at each reference point. Send all data to server and preprocess to build the *radio map*. Next is the online localization phase. At this time, we test the signal strength value for t times for each visible AP at each reference point. Log the real position as true result. Finally we compare the radio map and the tested RSS data and make the localization decision. Then we can get the ratio of correct localization result with all reference point as reliability.

7.1.1 Fingerprint Collection

Although fingerprinting localization method is popular by its free hardware deployment, it still has its most laborious job—collecting the training data. In order to do this, we write a simple RSS detection *JAVA* code for Android platform.

When collecting the training RSS data, we just need to place the phone at one of the reference point, enter the position ID of that reference point and also the collecting frequency and time, and click the start button and wait for the collecting procedure until it finished at this reference point. And move to the next position. After travelled all the reference point, we have finished the RSS collection procedure.

7.1.2 Database and Server

When the client sent the raw collected RSS data to server, we need to make a preprocess and build the radio map in the database. First step is to regular the data structure and save the fingerprint information into the database waiting for comparison with location request data. We both calculated the typical mean values of RSS as a kind of radio map, and we also calculate the temporal correlation of RSS as a secondary radio map. The calculation method is just as section 6.2 states.

7.1.3 Location Determination

As for the process of location determination, the comparison part for the report RSSes and radio map, we use basic k-nearest-neighborhoods to find the localization result. The determination algorithm is consist of "coarse localization" and "fine localization". As most of the work in the literature does, we first find a list of candidate locations of the user with the mean value comparison, which is named as "coarse localization". And then among all the candidate positions, we find the most likely location with the temporal correlation comparison as "fine localization". Through this two level of positioning, the accuracy of localization can be highly improved.

Of course, there are more accurate and evolved positioning algorithms so far, especially the machine learning algorithms, but algorithm is not the main consideration for this paper after all. So we only need to find a way out to prove the efficiency and effectiveness of temporal correlation of RSS for one algorithm for example is enough. And this is the reason why we do not need to further compare with the other experiment algorithms.

7.2 Trace-driven Simulation

In this section, we demonstrate this trace-driven simulation to show the performance difference between the system utilizing and the system ignoring temporal correlation of the RSS.

7.2.1 Simulation introduction

The system are conducted in a indoor environment to verify our analysis for the 1-D physical space. We use two mobile devices to measure the RSSes from one AP at two different locations that is 2 meters from each other. In order to differentiate temporal correlations of the two locations, we add noise of people motion to one of the channels from the AP to mobile devices. We measure the RSS value every 100 millisecond for 1k times at each location.

Traditional localization estimation processes extract the RSS information independently and build the corresponding PDF in the database, such as the measured RSS distribution shown in Fig. 7–1, where each curve represents the PDF of each location. The two figures represent

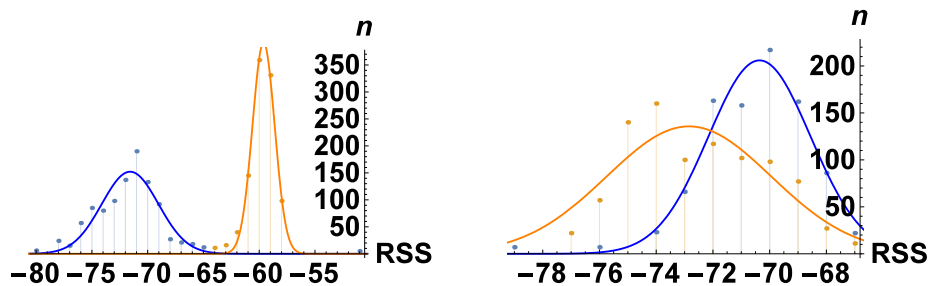


Figure 7–1: PDFs of the tested RSSes

two cases, where the first case means that the temporal correlation at each location is distinctive, and the second case means that the two locations' temporal correlations are similar to each other.

The regression parameters for the Gaussian PDFs are as shown in Table 7–1.

Table 7–1: RSS results fitting 1-d Gaussian parameters

Gaussian	Pic1_r1	Pic1_r2	Pic2_r1	Pic2_r2
A	152.119	391.278	205.92	135.665
μ	-71.574	-59.61	-70.3584	-72.8452
σ	3.5943	1.409	2.54672	4.10548

7.2.2 Simulation in 2-D PDFs with correlation

In order to present the trace-simulation of theoretical model, we use two dimensional probability density functions formed by real test RSS data pairs. In this way, the two dimensional temporal correlation can be well presented in such a two dimensional Gaussian distribution. Based on the fingerprints observed above, we now construct the corresponding 2-D temporal correlation PDFs, which are illustrated in Fig. 7-2 (a) and Fig. 7-2(b). The corresponding regression parameters for the joint 2-D Gaussian PDFs are shown in Table II.

Table 7-2: RSS results fitting 2-D Gaussian parameters.

Gaussian	Pic1_r1	Pic1_r2	Pic2_r1	Pic2_r2
A	126.274	254.858	184.975	124.457
μ	-71.5829	-59.5945	-70.3273	-72.8478
σ	2.5122	0.9905	1.7931	2.8962
ρ	0.9877	0.9215	0.977799	0.99263

The experimental results are shown in Fig. 7-2 (c) and Fig. 7-2 (d), where the blue and yellow dots are fingerprints reported at the first and the second locations, respectively. We can see from Fig. 7-2 (a), the blue dome-like function is the regression distribution of a less correlated position and the orange dome-like function is more correlated. The height of the 2-dimensional distribution is the count of that RSS pairs. The center of the distribution is actually the mean value of testing signal strength data. The situation of Fig. 7-2 (b) represents the two positions are not separated explicitly. In this case, the mean value of this two reference points are closer to each other and makes the matching process not accurate. So the temporal correlation information could be helpful.

Fig. 7-2 (c) and Fig. 7-2 (d) are the vertical view of Fig. 7-2 (a) and Fig. 7-2 (b) respectively. The curve and straight-line boundaries to separate dots are generated by the system considering and ignoring the temporal correlation. In both cases shown in Fig. 7-2 (c) and Fig. 7-2 (d), the curve boundary helps the system make more accurate location estimation. Due to the way of presentation, the seemingly one point on the figures actually represents many fingerprints. The results show that the number of fingerprints whose associated locations have been correctly estimated is much higher with the temporal boundary. We can expect that the

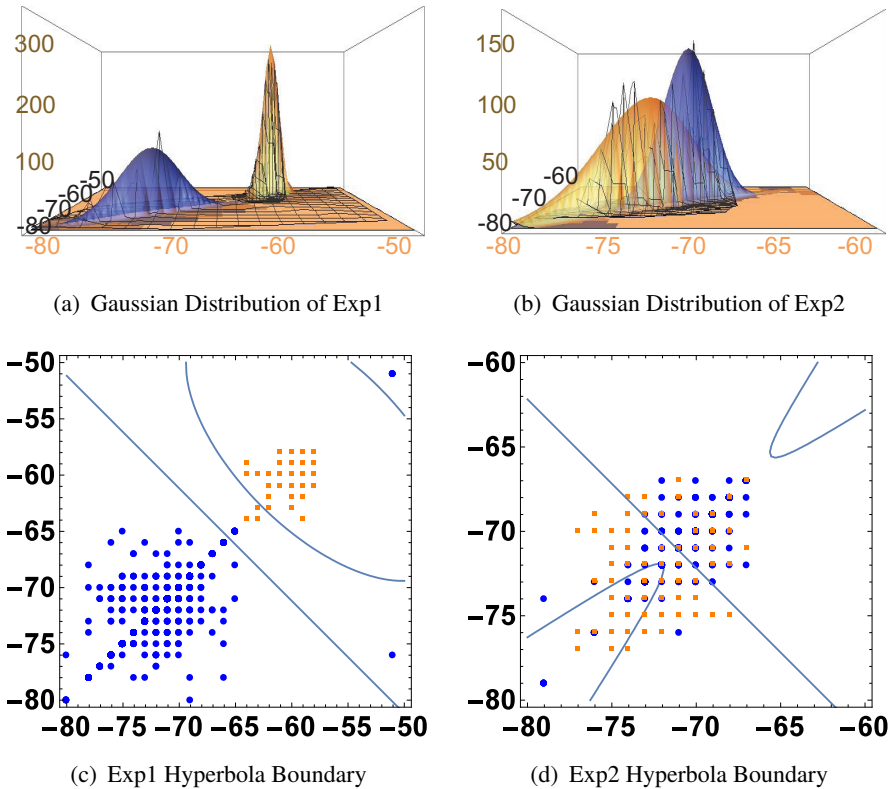


Figure 7-2: 2-D Gaussian Distribution and Hyperbolic Criteria for Localization

performance of the system will be better if more fingerprints are sampled. In order to deal with the small probability event, we put both of arms of the hyperbola in the figure. An interesting finding is that there is a blue dot in the upper right of Fig. 7-2 (c), which can be correctly localized with the temporal boundary.

This is the most simplest case for 2-dimensional temporal series and 1-dimensional physical space with only two reference points. However, sometimes the simpler case is easy to explain more clearly and reveal their echo with theoretical model. Regressed 2-dimensional Gaussian distribution with received signal strength pairs is the most direct way to present the multivariate Gaussian distribution model considering the temporal correlation. In this trace-driven simulation, we establish a direct connection between the theoretical modeling and experimental settings.

7.3 Evaluation and Experimental Results

This section shows how the temporal correlation information of the RSS could improve the performance of fingerprinting based localization in practice. We demonstrate the improvement of reliability given the different accuracy radius. In our system, we use the temporal correlation coefficient as an auxiliary reference information. Traditional positioning systems only use the information of mean value of the RSSes, the best accuracy of which is greater than 2 meters. We found when only adding one dimension of correlation, we can improve the reliability of the localization accuracy around 10%.

Our experimental area is around forty square meters, and we divided them into 10×10 60cm grids. In the fingerprint collecting phase, we collect the RSS data of all available Wi-Fi Access Points with 25ms for 4000 times at each position. After pre-processing of filtering the raw data, we calculate the mean and correlation coefficients of each position as their fingerprinting maps. In the location determination phase, we use the strongest five signal strength information with 25ms for 1500 times. And we deploy k Nearest Neighbors algorithm to find the most probable positions. In addition, we set a threshold Th for the kNN Euclidian distances between testing and fingerprint RSSes. Here we can find some l_{kmin} positions with distance smaller than the threshold Th . After that we use temporal correlation to make the final decision. We find the nearest position among that l_{kmin} positions in the temporal correlation space.

We use the value of μ and ρ with respect to different Access Points at each location as the local fingerprints in the localization database. At each sampling location, we collect totally 4000 RSS fingerprints at the sampling interval of $25ms$ with respect to each Wi-Fi AP available. In the localization phase, we sample totally 1500 fingerprints at the sampling interval of $25ms$, where the top 5 strongest fingerprints are sampled. We compare the mean value of the sampled fingerprints and those have been stored in the database with the K-nearest neighbors (KNN) algorithm. In particular, we find sampled RSSes' neighbors that are within a threshold Th in the sample space, and put the corresponding associated locations on a list. For each location on the list, we examine the corresponding correlation coefficient with that of the sampled RSSes. The location matched most will be determined as the estimated location of the user.

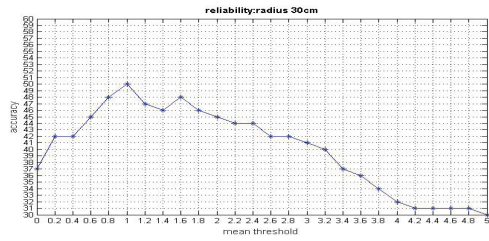
We evaluate the localization performance by considering both the accuracy and reliability. In the experiment, we first set an error tolerance radius δ , which means that any estimated locations within the δ neighborhood of the user's actual location can be regarded as a correct estimation. We set different radius and randomly pick up 500 estimations to evaluate the performance. With the results of localization, we could find the probability that the user's location is correctly estimated, which is termed as reliability.

We can easily find that the contribution weight of mean and rho in location determination phase is mainly determined by the distance threshold Th . What is the proper value should set on Th is an important factor for our system. As the pictures show, the mean threshold Th is ranging from 0 to 5, and the reliability is started growing and ended declining. With the accuracy radius ranges from 30cm to 3m, the reliability shows different scales of improvement as long as the threshold is smaller than 3.

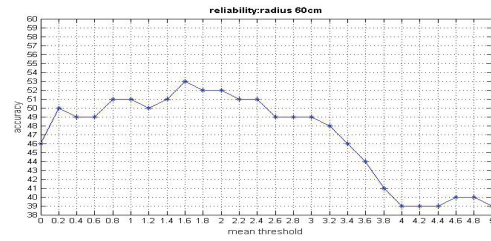
The experiment results are illustrated in Fig 7-3. The radius is set to be 30cm, 60cm, 120cm, 180cm, 210cm, 240cm, 270cm, 3000cm, respectively. In each case, we increase the threshold Th from 0 to 5 with increment of 0.2. Note that the unit of the threshold is not important, as we are consider the normalized distance in the sample space. As shown in Fig 7-3, the localization reliability increases first and then decreases as the threshold increases in all scenarios.

If the threshold is 0, the user's location is basically estimated using the mean of the RSSes; the information of the temporal correlation is not utilized. If the threshold increases, the system could cross check the candidate locations and find the most matched one; therefore the reliability is improved. If the threshold is large enough, it means that more candidate locations could be on the list. Since those locations are picked up according to their corresponding fingerprints in the sample space, they may be far away from each other in the physical space. Their observed temporal correlation information is unable to effectively tell one location from another. The more the candidate locations are, the higher probability that the location is far from the APs, and the temporal correlation becomes indistinguishable. That is why the reliability becomes worse if the threshold is too large.

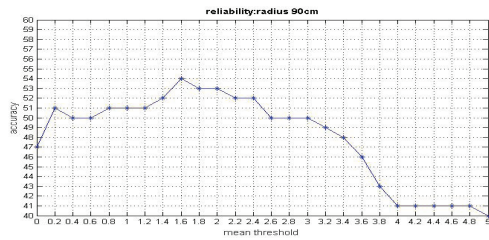
To further explore the experimental results, we will explain more about the details of the



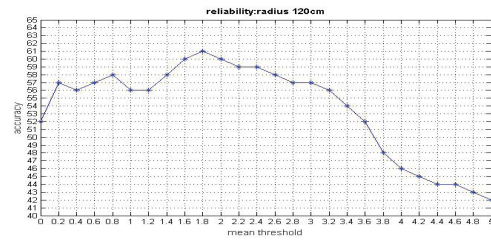
(a) Accuracy radius: 30cm



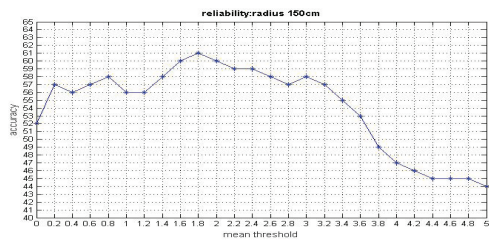
(b) Accuracy radius: 60cm



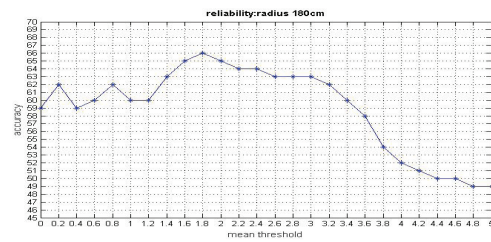
(c) Accuracy radius: 90cm



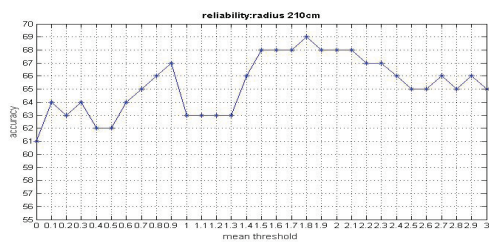
(d) Accuracy radius: 120cm



(e) Accuracy radius: 150cm



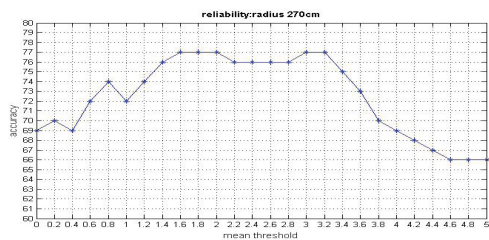
(f) Accuracy radius: 180cm



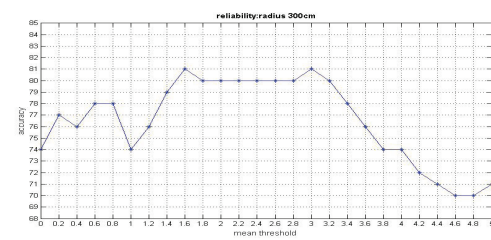
(g) Accuracy radius: 210cm



(h) Accuracy radius: 240cm



(i) Accuracy radius: 270cm



(j) Accuracy radius: 300cm

Figure 7-3: Reliability with different threshold H and error tolerance radius

figures. Firstly, we can see that intersection of y axis is actually the localization reliability without correlation information of signals. With utilizing mean value of RSS only, the localization reliability increased when the accuracy radius enlarged, from 37% to 74% as radius goes from 30 centimeters to 3 meters. And as the x variable threshold Th increases from 0 to 5, the reliability basically increased and then decreased with a little vibrations. As mentioned before, the threshold Th determine the ratio of influence between mean value and temporal correlation. The increment of Th means the temporal correlation information is making a bigger sense in location determination. We can see that the reliability would increase at the beginning and reach the maximum when Th is around 1.8, and then decrease more or less until less than the original value of reliability. We can also find that the larger accuracy radius is, the later of decrement is as Th growing. Although the trend is increasing at first and decreasing at last, the reliabilities with Th smaller than 3 are all larger than original value, which means that it can be guaranteed that the improvement of reliability within some interval. Another thing that we should notice is that, although the value of reliability is smaller when Th is large enough, this does not mean the temporal correlation would cause decrement of reliability. Furthermore, when accuracy radius is larger than 3 meters, the critical Th that caused decrement of reliability before would also make improvement when accuracy radius increased correspondingly. The experiment data are further analyzed as Table 7–3, which shows that the reliability of the fingerprinting localization could be improved by up to 13% if we choose the radius of 0.3m and the threshold of 1.

Table 7–3: Combination of H and radius and corresponding reliability improvement

Radius δ	Mean Threshold H	Reliability Improvement
0.3m	1	13%
0.6m	1.6	7%
0.9m	1.6	7%
1.2m	1.8	9%
1.5m	1.8	9%
1.8m	1.8	7%
2.1m	1.8	8%
2.4m	1.8	12%
2.7m	1.8	8%
3.0m	1.8	7%

SUMMARY

In this paper, we have theoretically shown that the temporal correlation of the RSS can further improve accuracy of the fingerprinting localization. In particular, we have constructed a theoretical framework to evaluate how the temporal correlation of the RSS can influence reliability of location estimation, which is based on a newly proposed radio propagation model considering the time-varying property of signals from Wi-Fi APs. The framework has been applied to analyze localization in the one dimensional physical space, which reveals the fundamental reason why localization performance can be improved by leveraging temporal correlation of the RSS. We have extended our analysis to high-dimensional scenarios and mathematically depict the boundaries in the RSS sample space, which distinguish one physical location from another. Moreover, we have developed an algorithm to utilize temporal correlation of the RSS to improve the location estimation accuracy, where the process for choosing key design parameters are provided through experiments. Experiment results show that the localization accuracy can be improved by up to 13% with appropriate leveraging the RSS temporal correlation.

Our future work is mainly to consider how to refine our model with other signal strength distributions, like Multi-Gaussian, multimodal scenarios. Another interesting thing is to fix the different hardware problem and pedestrian motion influence. How to build a model properly describe the version control and temporal difference would be very useful in localization system. And the positioning algorithms utilizing temporal correlation of signal can be further improved.

There is a still long way to go before a standard indoor localization system can be formed, and there are kinds of problems to solve in each step of the positioning procedure, like fingerprint-collecting, RP deployment, AP selection, positioning algorithms and so on. Besides solving the system problems and improve its performance practically, we also need to find their mathematical mechanism by theoretical analysis at the same time, which can always lead the development of the real systems in a correct and efficient way.

Bibliography

- [1] Z. Zhou Z. Yang and Y. Liu. “From RSSI to CSI: Indoor localization via channel response”. In: *ACM Computer Survey* 46.2 (2013), pp. 1–32.
- [2] J. Yang S. Sidhom Y. Wang Y. Chen H. Liu Y. Gan and F. Ye. “Push the Limit of WiFi based Localization for Smartphones”. In: *Proc. ACM MobiCom*. ACM. 2012, pp. 305–316.
- [3] S. Sidhom Y. Wang Y. Chen H. Liu J. Yang and F. Ye. “Accurate WiFi Based Localization for Smartphones Using Peer Assistance”. In: *IEEE Transactions on Mobile Computing* 13.10 (2013), pp. 2199–2214.
- [4] V. N. Padmanabhan A. Rai K. K. Chintalapudi and R. Sen. “Push the Limit of WiFi based Localization for Smartphones”. In: *Proc. ACM MobiCom*. ACM. 2012, pp. 293–304.
- [5] B. Lu S. Fang and Y. Hsu. “Learning location from sequential signal strength based on GSM experimental data”. In: *IEEE Transactions on Vehicular Technology* 61.2 (2012), pp. 726–736.
- [6] S. Fang and T. Lin. “A dynamic system approach for radio location fingerprinting in wireless local area networks”. In: *IEEE Transactions on Communications* 58.4 (2010), pp. 1020–1025.
- [7] S. Kuo and Y. Tseng. “A scrambling method for fingerprint positioning based on temporal diversity and spatial dependency”. In: *IEEE Transactions on Knowledge and Data Engineering* 20.5 (2008), pp. 678–684.
- [8] J. Yang S Liu Y. Chen M. Gruteser G. Chandrasekaran M. A. Ergin and R. P. Martin. “Empirical evaluation of the limits on localization using signal strength”. In: *Proc. IEEE SECON*. IEEE. 2009, pp. 1–9.

- [9] S. Kyperountas I. Hero A.O. R. Moses N. Patwari J. Ash and N. Correal. “Locating the nodes: cooperative localization in wireless sensor networks”. In: *IEEE Signal Processing Magazine* 22.4 (2005), pp. 55–69.
- [10] M. Perkins N. S. Correal N. Patwari A. O. H. III and R. J. O’dea. “Relative location estimation in wireless sensor networks”. In: *IEEE Transactions on Signal Processing* 51.8 (2003), pp. 2137–2148.
- [11] V. Atanasovski M. Angjelichinoski D. Denkovski and L. Gavrilovska. “Cramér-Rao Lower Bounds of RSS-Based Localization With Anchor Position Uncertainty”. In: *IEEE Transactions on Information Theory* 61.5 (2015), pp. 2807–2834.
- [12] A. Padmanabha Iyer K. Chintalapudi and V. N. Padmanabhan. “Indoor localization without the pain”. In: *Proc. ACM MobiCom*. ACM. 2010, pp. 173–184.
- [13] X. Wang Y. Wen X. Tian and S. Lu. “Fundamental limits of RSS fingerprinting based indoor localization”. In: *Proc. IEEE INFOCOM*. IEEE. 2015, pp. 2479–2487.
- [14] E. Martínez M. Rodríguez J. Favela and M. Muñoz. “Location-aware access to hospital information and services”. In: *Information Technology in Biomedicine, IEEE Transactions on* 8.4 (2004), pp. 448–455.
- [15] Hamid Harroud, Mohamed Ahmed, and Ahmed Karmouch. “Policy-driven personalized multimedia services for mobile users”. In: *Mobile Computing, IEEE Transactions on* 2.1 (2003), pp. 16–24.
- [16] T. Lin S. Fang and K. Lee. “A novel algorithm for multipath fingerprinting in indoor WLAN environments”. In: *Wireless Communications, IEEE Transactions on* 7.9 (2008), pp. 3579–3588.
- [17] V. Ranki F. Belloni P. Kemppi T. Rautiainen and J. Pajunen. “Hybrid positioning system combining angle-based localization, pedestrian dead reckoning and map filtering”. In: *Indoor Positioning and Indoor Navigation (IPIN), 2010 International Conference on*. IEEE. 2010, pp. 1–7.

- [18] E. Servan-Schreiber T. Hodes R. Katz and L. Rowe. “Composable ad-hoc mobile services for universal interaction”. In: *Proceedings of the 3rd annual ACM/IEEE international conference on Mobile computing and networking*. ACM. 1997, pp. 1–12.
- [19] U. Bandara, H. Morikawa M. Hasegawa M. Inoue, and T. Aoyama. “Design and implementation of a bluetooth signal strength based location sensing system”. In: *Radio and Wireless Conference, 2004 IEEE*. IEEE. 2004, pp. 319–322.
- [20] V. Falcao R. Want A. Hopper and J. Gibbons. “The active badge location system”. In: *ACM Transactions on Information Systems (TOIS)* 10.1 (1992), pp. 91–102.
- [21] R. Peng and M. Sichitiu. “Angle of arrival localization for wireless sensor networks”. In: *Sensor and Ad Hoc Communications and Networks, 2006. SECON’06. 2006 3rd Annual IEEE Communications Society on*. Vol. 1. IEEE. 2006, pp. 374–382.
- [22] H. So Y. Chan W. Tsui and P. Ching. “Time-of-arrival based localization under NLOS conditions”. In: *Vehicular Technology, IEEE Transactions on* 55.1 (2006), pp. 17–24.
- [23] A. Haimovich C. Comşa J. Luo and S. Schwartz. “Wireless localization using time difference of arrival in narrow-band multipath systems”. In: *Signals, Circuits and Systems, 2007. ISSCS 2007. International Symposium on*. Vol. 2. IEEE. 2007, pp. 1–4.
- [24] V. Padmanabhan A. Rai K. Chintalapudi and R. Sen. “Zee: zero-effort crowdsourcing for indoor localization”. In: *Proceedings of the 18th annual international conference on Mobile computing and networking*. ACM. 2012, pp. 293–304.
- [25] A. Elgohary-M. Farid M. Youssef H. Wang S. Sen and R. Choudhury. “No need to war-drive: unsupervised indoor localization”. In: *Proceedings of the 10th international conference on Mobile systems, applications, and services*. ACM. 2012, pp. 197–210.
- [26] D. Katabi S. Kumar S. Gil and D. Rus. “Accurate indoor localization with zero start-up cost”. In: *Proc. ACM MobiCom*. ACM. 2014, pp. 483–494.
- [27] A. Agrawala M. Youssef and S. Udaya. “WLAN location determination via clustering and probability distributions”. In: *Pervasive Computing and Communications, 2003.(PerCom*

- 2003). *Proceedings of the First IEEE International Conference on*. IEEE. 2003, pp. 143–150.
- [28] K. Plataniotis A. Kushki and A. Venetsanopoulos. “Kernel-based positioning in wireless local area networks”. In: *Mobile Computing, IEEE Transactions on* 6.6 (2007), pp. 689–705.
- [29] W. Valaee C. Feng W. Au and Z. Tan. “Received-signal-strength-based indoor positioning using compressive sensing”. In: *Mobile Computing, IEEE Transactions on* 11.12 (2012), pp. 1983–1993.
- [30] S. Kumar D. Vasisht and D. Katabi. “Decimeter-Level location with a single WiFi access point”. In: *Proc. NSDI*. 2016, pp. 165–178.
- [31] A. Padmanabha Iyer K. Chintalapudi and V. N. Padmanabhan. “SpotFi: Decimeter level localization using WiFi”. In: *Proc. ACM SIGCOMM*. ACM. 2015, pp. 269–282.
- [32] A. Sheth D. Halperin W. Hu and D. Wetherall. “Tool release: Gathering 802.11n traces with channel state information”. In: *Proc. ACM SIGCOMM CCR* 41.1 (2011), pp. 53–53.
- [33] K. Kaemarungsi and P. Krishnamurthy. “Properties of indoor received signal strength for WLAN location fingerprinting”. In: *Mobile and Ubiquitous Systems: Networking and Services (MOBIQUITOUS)*. IEEE. 2004, pp. 14–23.
- [34] M. Youssef and A. Agrawala. “Handling samples correlation in the horus system”. In: *INFOCOM 2004. Twenty-third Annual Joint Conference of the IEEE Computer and Communications Societies*. Vol. 2. IEEE. 2004, pp. 1023–1031.
- [35] K. Kaemarungsi and P. Krishnamurthy. “Modeling of indoor positioning systems based on location fingerprinting”. In: *Proc. IEEE INFOCOM*. IEEE. 2004, pp. 1012–1022.
- [36] X. Li E. Elnahrawy and R. P. Martin. “The limits of localization using signal strength: A comparative study”. In: *Proc. IEEE SECON*. IEEE. 2004, pp. 406–414.
- [37] L. D. Branges. “The Stone-Weierstrass theorem”. In: *Proceedings of the American Mathematical Society* 10.5 (1959), pp. 822–824.